

The Nature of the Young Supernova Remnant S8 in the Dwarf Galaxy IC 1613

ROBERT A. FESEN¹ AND KATHRYN E. WEIL¹

¹6127 Wilder Lab, Department of Physics and Astronomy, Dartmouth College, Hanover, NH 03755 USA

ABSTRACT

We present sub-arcsecond optical images and low- to moderate-resolution spectra of the compact, X-ray and optically bright supernova remnant known as S8 in the nearby dwarf galaxy IC 1613. Deep H α images of the remnant show a sharply defined crescent shaped nebula, while narrow passband images reveal a coincident and unexpectedly bright continuum nebulosity exhibiting a size and morphology like that seen for the remnant’s line emissions. Low-dispersion spectra covering 3600 – 9000 Å show numerous low-ionization line emissions such as [O I] and [Fe II], along with higher-ionization emission lines including He II and optical coronal lines [Fe VII], [Fe X], [Fe XI], and [Fe XIV]. This suggests the presence of a wide range of shock velocities from ~ 50 to over 350 km s^{-1} , corresponding to preshock densities of $\sim 1 - 30 \text{ cm}^{-3}$. Higher resolution spectra indicate an expansion velocity around 180 km s^{-1} with a $\sim 45 \text{ km s}^{-1}$ wide central cavity. H α emission spans rest frame velocities of $+120$ to -240 km s^{-1} and we estimate a total nebula mass of $119 \pm 34 M_{\odot}$. We conclude S8 is a relatively young supernova remnant ($\simeq 2700 - 4400 \text{ yr}$) exhibiting properties remarkably like those seen in the young LMC remnant N49, including age, physical size, shock velocities, filament densities, optical line strengths, X-ray and optical luminosities, and coronal line and continuum emissions.

Keywords: SN: individual objects: ISM: supernova remnant

1. INTRODUCTION

Studies of young core-collapse supernovae (CCSNe) remnants are useful for understanding high mass stellar explosions, ejecta asymmetries, and the formation of central compact objects (Chevalier 2005; Patnaude & Badenes 2017). Unfortunately, young CCSN remnants with ages less than about 5000 yr are relatively rare as there are only about a dozen known in the Milky Way, and just a few more in the Magellanic Clouds and other extragalactic systems (Milisavljevic & Fesen 2017; Branch & Wheeler 2017).

One of the few suspected young extragalactic supernova remnants (SNRs) is a small compact remnant, S8, located in the outskirts of the Local Group dwarf irregular galaxy IC 1613 ($d = 725 \text{ kpc}$; Hatt et al. 2017). Labeled by Sandage (1971) as emission nebula No. 8 in IC 1613, hence the name S8, it was initially seen as just one of several H II regions in the northeastern region of IC 1613. However, it was subsequently recognized as a SNR based on optical emission line ratios and nonthermal radio flux index (Smith 1975; Dodorico et al. 1980; Dickel et al. 1985; Peimbert et al. 1988).

Classified as a small composite SNR consisting of a bright radio and optical emission shell and an X-ray bright extended nebula (Schlegel et al. 2019), the remnant appears in the optical as a bright crescent shaped emission nebula $3''.5 \times 5''.0$ in size ($12 \text{ pc} \times 18 \text{ pc}$ at 725 kpc) Its optical spectra have been modeled with shock velocities $\sim 50\text{--}150 \text{ km s}^{-1}$. It exhibits an expansion ve-

locity of $250\text{--}300 \text{ km s}^{-1}$, low metallicity reflective of IC 1613’s abundances, and [S II] line emissions indicating a relatively high electron density of $\simeq 1400 \text{ cm}^{-3}$, consistent with a young remnant (Lozinskaya et al. 1998; Lozinskaya & Podorvanyuk 2009).

With an estimated age of $\sim 3400\text{--}5600 \text{ yr}$, the S8 remnant is quite luminous in the optical and X-rays, with an X-ray luminosity of $5.6 \times 10^{36} \text{ erg s}^{-1}$ (Schlegel et al. 2019) ranking it among the brightest X-ray SNRs in the Local Group. It is also bright in the radio, with a luminosity nearly 20% that of the Crab Nebula at 20 cm, with a spectral index of -0.56 ± 0.06 consistent with a SNR’s nonthermal emission associated with ISM shocks (Lozinskaya et al. 1998). Given its location in among IC 1613’s northeastern H II regions and large superbubbles, formed via stellar winds from massive stars, plus its size and X-ray luminosity S8 is a suspected CCSN remnant (Rosado et al. 2001; Ou et al. 2018; Schlegel et al. 2019).

Due to its suspected youth, high luminosity and expansion velocity, S8 has been compared to some young LMC core-collapse SNRs (Lozinskaya et al. 1998; Schlegel et al. 2019). Here we present sub-arcsecond H α and continuum filter images along with low and moderate resolution optical spectra of the S8 remnant obtained in order to explore its optical properties and hence its nature in relation to other relatively young SNRs. Our data are described and presented in §2 and §3. In §4, we discuss this remnant’s general optical properties, possible origins of its unusually bright and extended contin-

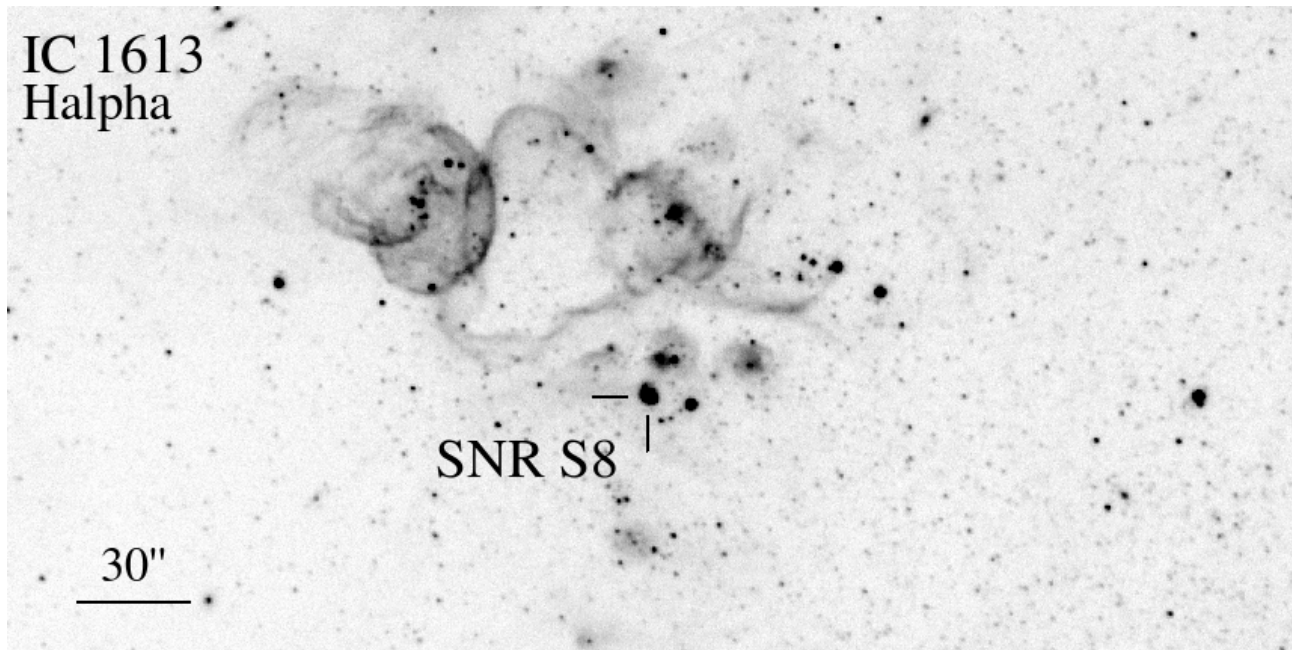


Figure 1. $H\alpha$ image of the H II regions in the northern area of IC 1613 around the location of the supernova remnant S8. North is up, East is to the left.

uum emission, and compare its optical and X-ray properties to young CCSN remnants in the LMC and nearby galaxies.

2. OBSERVATIONS

A series of both broad and narrow passband interference filter images of SNR S8 were obtained in October 2019 and January 2020 with the 2.4m Hiltner telescope at the MDM Observatory at Kitt Peak, Arizona using the Ohio State Multi-Object Spectrograph (OSMOS; Martini et al. 2011). Images were taken using a V band filter, an [O III] 5007 Å filter (FWHM = 80 Å), an $H\alpha$ filter (FWHM = 80 Å), and a broadband R filter matching that of the ACS F675W filter aboard the *Hubble Space Telescope* (*HST*). Additional images were taken using narrow passband filters centered on spectral regions free of any of S8’s strong line emissions based on previously published spectra (Peimbert et al. 1988; Lozinskaya et al. 1998). These continuum filter images included a blue continuum filter ($\lambda_c = 5288$ Å, FWHM = 256 Å), and two red continuum filters centered on either side of $H\alpha$; $\lambda_c = 6071$ Å (FWHM = 260 Å), and $\lambda_c = 7021$ Å (FWHM = 177 Å). Multiple exposures were taken in each filter with exposures ranging from 30 s for the F675W filter to 1200 s for the narrow passband filters. Seeing was very good for most images, with measured FWHM values for individual 7021 Å filter images ranging between $0''.80 - 0''.84$ and $0''.90 - 0''.95$ for $H\alpha$ images.

We note that the 6071 Å continuum filter’s transmission window covers an almost completely emission line free portion of the remnant’s optical spectrum (see §3.2

below). The filter’s transmission curve has sharp cut-on/cut-offs at 5900 and 6200 Å, meaning that with the exception of weak [Fe VII] 6087 Å emission, the filter provides a ~ 300 Å wide emission line free bandpass. Similarly, the 7021 Å filter’s bandpass of ~ 250 Å (6900 to 7150 Å) is sensitive to only He I 7065, [Ar III], and [Fe II] 7155 which are relatively weak in S8 (see §3.2 below).

Images taken in October 2019 were followed by a series of low dispersion, long-slit OSMOS spectra using two different grism setups. Using a 1.4 arcsec N-S slit and a red VPH grism ($R = 1600$), we obtained 2×2000 s spectra covering 4500–8500 Å with a measured FWHM $\simeq 6.5$ Å. This was followed by two blue VPH grism setups using a 1.2 arcsec slit and covering the wavelength regions 3600–5900 and 4000–7000 Å (FWHM = 3.5 Å). Exposure times ranged from 1200 to 3000 seconds. The resulting spectra were wavelength corrected by -230 km s^{-1} based on the measured rest velocity local H II regions, in close agreement with the galaxy center’s heliocentric velocity of -234 km s^{-1} (Lu et al. 1993).

In addition, we obtained moderate dispersion spectra ($R \simeq 12,400$) of the S8 remnant in January 2020 with the MDM 1.3m McGraw-Hill telescope using a Boller & Chivens Spectrograph (CCDS) in order to investigate the remnant’s velocity structure in finer detail. This spectrograph uses a Loral 1200×800 CCD detector. A 1800 grooves mm^{-1} grating blazed at 4700 Å was used to yield a wavelength coverage of 330 Å. Three 1500 seconds exposures were taken centered on the remnant’s $H\alpha$ emission under 1.5 – 2.0 arcsec seeing conditions. With a spectral scale of 0.265 Å per pixel and a measured comparison lamp resolution of 2.0 pixels using a

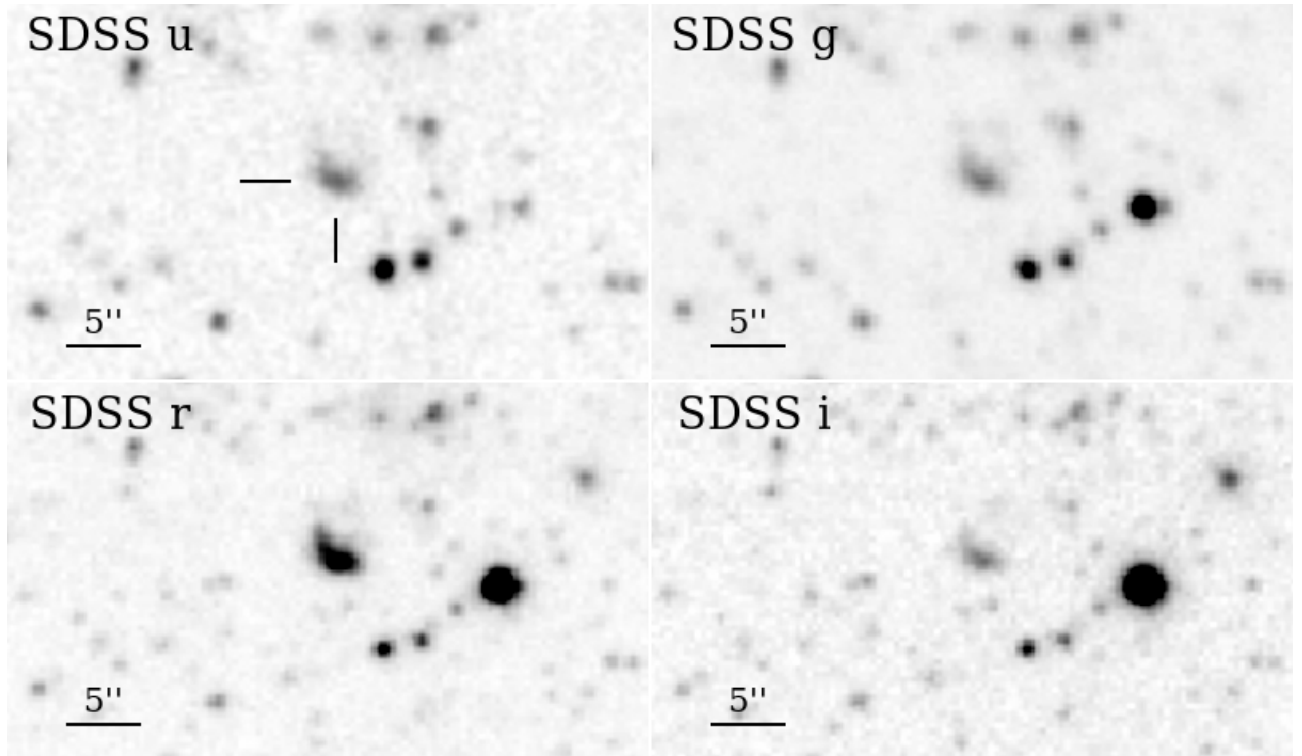


Figure 2. Sloan images of the IC 1613 supernova remnant S8, marked in the u band image. North is up, East is to the left.

1.5 arcsec wide slit, this set-up gave a velocity resolution of $\simeq 24 \text{ km s}^{-1}$ at $\text{H}\alpha$. This resolution was viewed adequate to explore the remnant’s $\text{H}\alpha$ emission velocity considering the remnant’s reported 250 to 300 km s^{-1} expansion (Lozinskaya et al. 1998; Lozinskaya & Podorvanyuk 2009).

Standard pipeline data reduction of both images and spectra made use of AstroPy and PYRAF¹. None of the October 2019 or January 2020 nights were strictly photometric, with occasional light and variable cirrus. Spectra were reduced using the software L.A. Cosmic (van Dokkum 2001) to remove cosmic rays. Spectra were calibrated using Ne, Xe, and Ar lamps and spectroscopic standard stars (Oke 1974; Massey & Gronwall 1990).

3. RESULTS

3.1. Image Data

As shown in Figure 1, the S8 remnant lies at the southern edge of a cluster of H II regions and large emission shells located in the northeastern outskirts of the IC 1613 galaxy. S8 is the only known SNR in the galaxy and has the highest surface brightness of any emission line nebula in IC 1613 (Lozinskaya et al. 1998). IC 1613 is located at a fairly high Galactic latitude (-60.6°) with a low estimated foreground Galactic extinction ($E(B - V) = 0.025$; Schlafly & Finkbeiner 2011).

Although several *HST* observing programs imaged parts of IC 1613, none covered the S8 site which might have informed us about the remnant’s fine-scale emission structure. Outside of Sandage’s initial $\text{H}\alpha$ image, there are also few high-resolution images of the S8 remnant in the literature (e.g., Lozinskaya et al. 1998; Rosado et al. 2001). Consequently, we investigated the remnant’s appearance both through archival optical survey data plus our new imaging data.

Broadband images of the S8 remnant are shown in Figure 2 where we present Sloan u,g,r,i images. In these images, the remnant exhibits a distinct crescent shape $3''.5 \times 5''.0$ in size toward the southeast, consistent with the size cited by Sandage (1971). The crescent is significantly brighter in its southwest corner, except in the u band where it appears more uniform in brightness. Our V band and F675W images matches that seen in the Sloan g and r images.

With the exception of the Sloan r band image, the remnant’s total flux is remarkably steady in the u,g, and i band images suggesting a relatively flat SED. Estimated remnant ugr magnitudes of 18.6, 18.7, 17.5, and 18.8 mag (± 0.15 mag) using neighboring stars in the Sloan DR16 database support this conclusion. S8’s bright appearance in the r band is likely due to that filter’s sensitivity to the remnant’s strong $\text{H}\alpha$, [O I] 6300, 6364 Å, [N II] 6548, 6583 Å, and [S II] 6716, 6731 Å line emissions.

However, the remnant’s bright appearance in Sloan i band is surprising. Previous spectra of the SNR along

¹ PYRAF is a product of the Space Telescope Science Institute, which is operated by AURA for NASA.

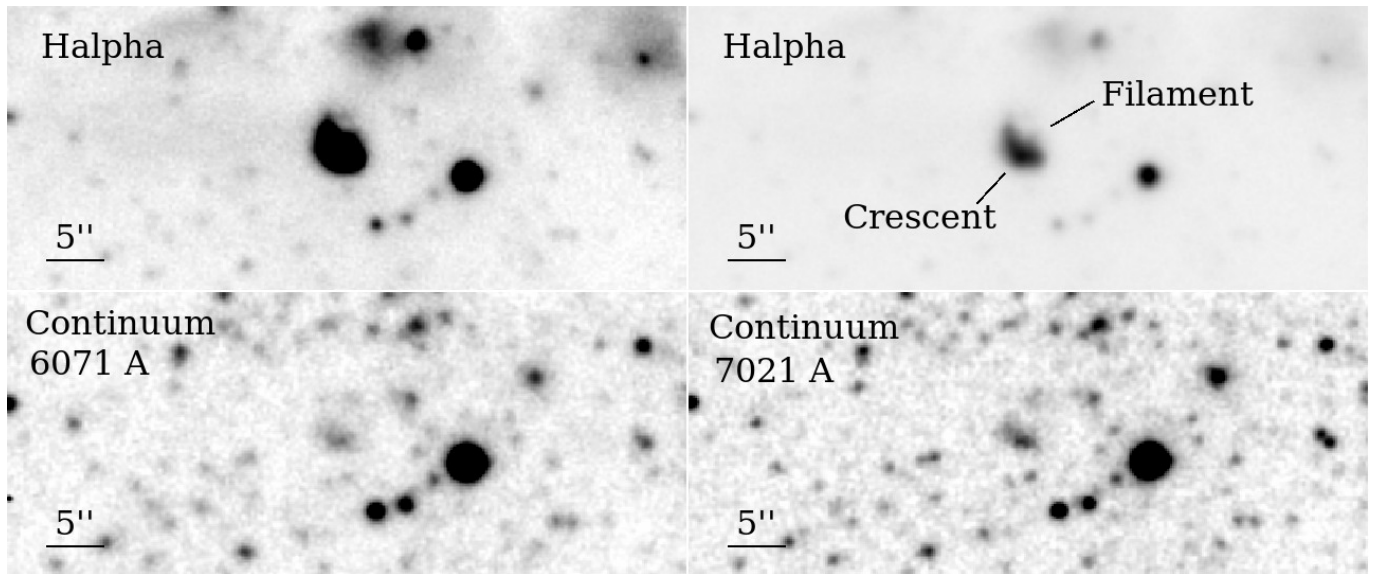


Figure 3. Top Panels: $H\alpha$ images of the S8 remnant; left panel shows its full extent in $H\alpha$ while the right panel presents a lower contrast version which better reveals the overall morphology including a single, interior filament. Lower Panels: Red continuum images ($\lambda_c = 6071$ and 7021 Å) showing the presence of continuum emission with a morphology similar to that of the remnant’s $H\alpha$ emission. North is up, East is to the left.

with our own spectra (see §3.2 below) show that S8 emits no strong emission lines in the Sloan i filter’s $\sim 7000 - 8500$ Å bandpass (Peimbert et al. 1988; Lozinskaya et al. 1998). The same is also true for the Sloan u band image where the filter’s bandpass is sensitive only to the remnant’s only modest strength [O II] 3726, 3729 Å emission.

Typically, evolved SNRs are mainly emission line nebulae and do not exhibit significant continuum emission, with the Crab Nebula being one of the few and most notable exceptions. Thus, the detection of the S8 remnant in the Sloan u and i band images was unexpected. This led us to obtain several narrow passband filter images to explore the remnant’s continuum emission and morphology.

In Figure 3, we present our sub-arcsecond $H\alpha$ and continuum images of S8, with the upper panels showing the remnant’s $H\alpha$ emission while the lower panels show the remnant’s continuum emission structure. The top left-hand panel shows the remnant’s full $H\alpha$ emission extent where it appears as a bright and sharply defined, thick crescent shaped nebula, along with possible faint diffuse extension to the northeast. Its elliptical shape has angular dimensions $\simeq 3''.5 \times 5''.0$, with a major axis at PA = $\simeq 30^\circ$. These numbers are considerably smaller than the $6'' \times 8''$ cited by Lozinskaya et al. (1998) and Rosado et al. (2001) but in good agreement with the major diameter of $5''.4$ reported by Sandage (1971) and Peimbert et al. (1988). An angular size of a $3''.5 \times 5''.0$ translates to 12 pc x 18 pc at 725 kpc.

The top right panel shows a lower contrast version of this same $H\alpha$ image emphasizing the elongated crescent shape of its brightest emission, along with a small, \sim

$1''.5$ long filament-like feature sticking out of its northern boundary. An [O III] filter image (not shown) presents a nearly identical size and morphology to that seen in $H\alpha$, consistent with previous emission line image results (Lozinskaya et al. 1998).

Both red continuum filter images, centered at 6071 and 7021 Å, reveal coincident and unexpectedly bright continuum nebosity exhibiting a size and morphology like that seen for the remnant’s line emissions. This continuum emission is best resolved in the 7021 Å filter image (FWHM = $0''.82$). This continuum emission appears diffuse with no clear evidence for the presence of one or more point sources. Consistent with the Sloan images, the remnant’s continuum is brightest toward the southwest and we estimate the peak brightness in the 6071 Å continuum filter to be $\sim 4-5\%$ that of $H\alpha$.

3.2. Low-Dispersion Spectra

3.2.1. Optical Spectral Properties of S8

Our low-dispersion spectrum of the S8 SNR covering the wavelength range of 3600 to 9000 Å is shown in Figure 4, with enlarged plots shown in Figure 5. These figures show the remnant’s full optical spectrum clearly for the first time, with as good or better S/N and spectral resolution than previously available. (Note: Faint continuum emission was detected but is too weak to see in this plot.)

Our spectrum is in general agreement with earlier published data and this is reflected in Table 1, where we compare our observed and extinction corrected relative line intensities for most of the stronger lines with those of previous works. Columns 1 and 2 list the observed line strengths for the S8 remnant from Dodorico & Do-

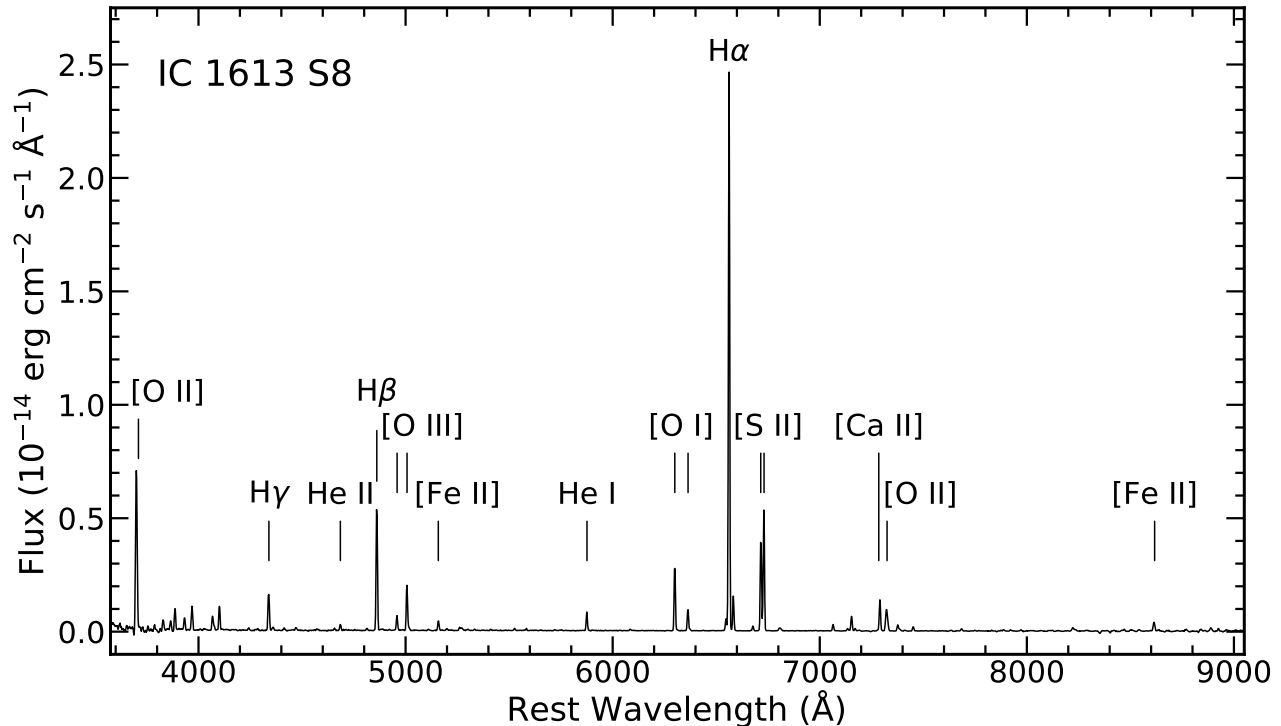


Figure 4. Observed optical spectrum of the S8 remnant.

pita (1983) and Lozinskaya et al. (1998), our observed and extinction corrected values in Columns 3 and 4, and extinction corrected line strengths from Peimbert et al. (1988) and Dopita et al. (2019) in Columns 5 & 6. We chose to list relative line strengths from previous and our own measurements in this way, to more easily show the consistency of our results with prior works for both the SNR’s main emission lines (Cols. 1 - 3) and the major and minor emission lines in the longer line lists of Peimbert et al. (1988) and Dopita et al. (2019) (Cols. 4 - 6).

IC 1613 has a low amount of foreground and internal reddening ($E(B - V) = 0.02$; Saha et al. 1992; Lee et al. 1993), with H II region spectral observations indicating $E(B - V) = 0.10$ (Lee et al. 2003). Based on our observed $H\alpha/H\beta$ ratio of 4.20, we calculated an $E(B - V) = 0.34$, equivalent to a value of $c \approx 0.44$, assuming an intrinsic ratio of 3.0 and an R value of 3.1 which has been shown to be valid for IC 1613 (Pietrzyński et al. 2006). We chose an $H\alpha/H\beta$ value greater than the theoretical value of 2.87 for 10^4 K due to the likelihood of significant collisional excitation of the $n = 3$ level at postshock temperatures seen in SNRs. Our extinction value is different from that of previous observers, which themselves differ from one another, and this may reflect real extinction differences internal to the remnant as suggested by variations in observed $H\alpha/H\beta$ ratios reported by Lozinskaya et al. (1998).

Even a casual inspection of the S8’s emission line strengths makes immediately obvious the weakness of

the metal lines of [O II] and [O III] 4959, 5007 line emissions relative to $H\beta$, the weakness of the [N II] 6548, 6583 lines, and [S II] 6716, 6731 relative to $H\alpha$ compared to Galactic SNRs. In Galactic SNRs as well as those in M31, M33, and other massive galaxies, [O III] is usually stronger and often much stronger than $H\beta$, with the [N II] 6583 line usually comparable to that of $H\alpha$. However in S8 these lines are relatively weak. The S8 spectrum carries clear signs of low metal ISM abundances like that seen in the Magellanic Clouds, not surprising given IC 1613’s estimated metallicity of $0.04 - 0.13 Z_{\odot}$ (Kingsburgh & Barlow 1995; Peimbert et al. 1988; Skillman et al. 2003; Garcia et al. 2014; Berger et al. 2018). In Table 1, we also include lists of published relative emission line strengths for two young core-collapse LMC remnants, namely N49 and N63A, which are discussed in relation to S8 in §4.2.

3.2.2. Electron Densities and Temperatures

The ratio of the [S II] 6716, 6731 lines can be used to estimate the electron density in the S^+ recombination zone and is nearly independent of electron temperature (Osterbrock & Ferland 2006). As shown in Table 1, both Dodorico & Dopita (1983) and Lozinskaya et al. (1998) reported the 6716/6731 ratio ≈ 0.80 , whereas Peimbert et al. (1988) and Dopita et al. (2019) find somewhat lower values of 0.78 and 0.77, respectively. While Peimbert et al. (1988) estimated an electron density, n_e , of $1500 \pm 230 \text{ cm}^{-3}$. Lozinskaya et al. (1998) estimated of $\approx 1300 \text{ cm}^{-3}$ based on an average ratio of 0.80 ± 0.05

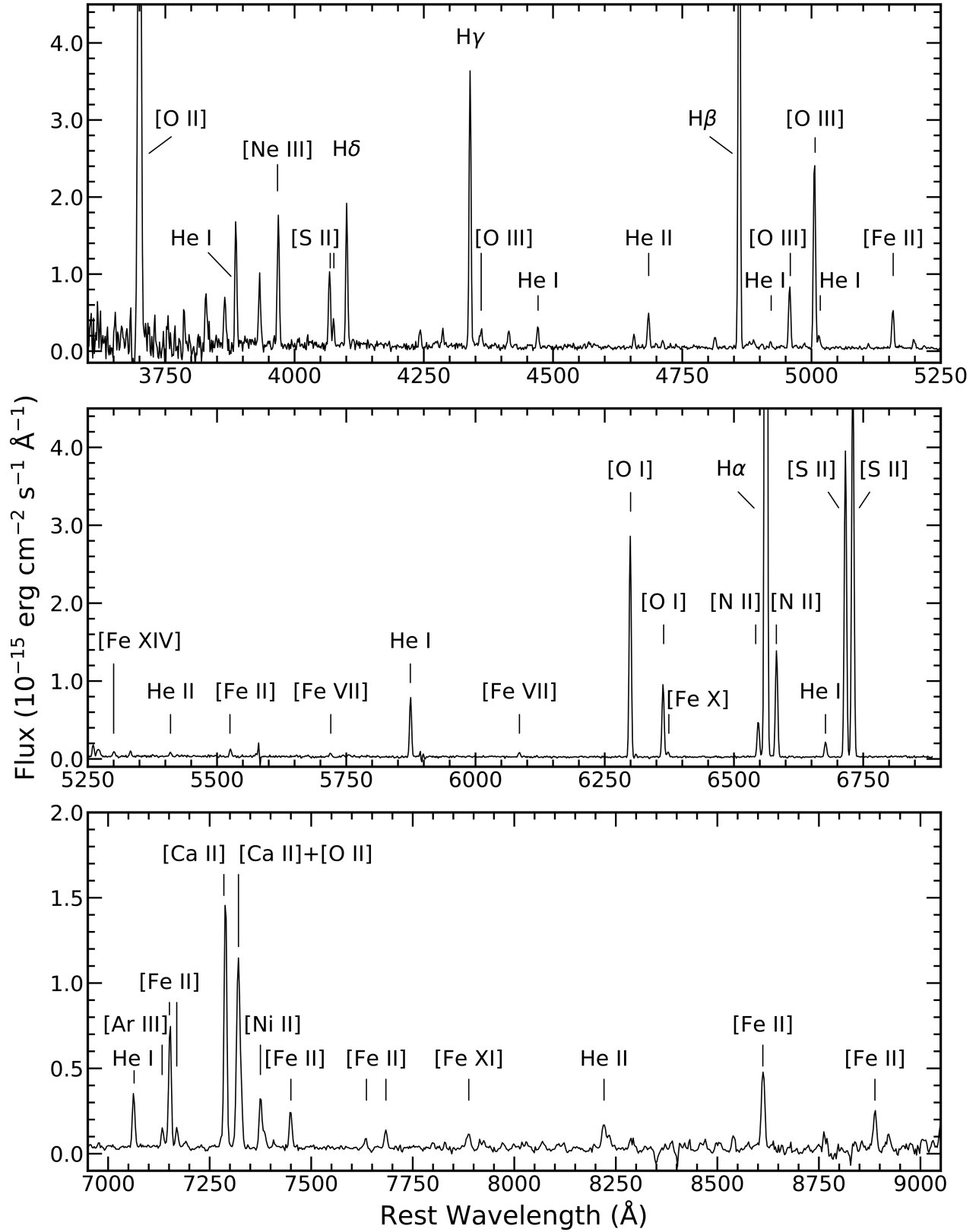


Figure 5. Enlargements of the observed spectra of the S8 remnant covering the 3600–5250 \AA , the 5250–6900 \AA , and the 6900–9000 \AA regions. Note the presence of faint [Fe VII] 5721, 6087, [Fe X] 6374, [Fe XI] 7892, and [Fe XIV] 5303 line emissions.

Table 1. Emission Line Strengths of S8 Compared to Previous Results and the LMC SNRs N49 and N63A

Emission Line (Å)	S8						N49	N63A
	DD83	L98	this work	this work	Peimbert88	Dopita19	Dopita19	RD90
	F(λ)	F(λ)	F(λ)	I(λ)	I(λ)	I(λ)	I(λ)	I(λ)
[O II] 3727	107.0	...	125	168	136.0	148.2	562.4	368.9
[Ne III] 3869	5.6	7.6	8.1	9.1	37.0	11.8
He I + H I 3889	13.8	18.7	18.6	19.0	22.1	18.6
[Ca II] 3934	8.0	11.5	10.0	10.6	15.6	8.2
[Ne III] 3967	14.0	18.0	24.0	22.6	33.3	24.5
[S II] 4068, 4076	15.0	...	11.6	17.1	17.8	17.7	39.3	29.1
Hδ 4102	18.0	...	16.1	21.2	25.1	24.0	25.2	26.6
Hγ 4340	35.0	35.0	32.8	38.9	45.7	46.1	45.4	44.4
[O III] 4363	2.0	5.0	2.3	2.7	4.0	3.1	3.9	...
He I 4472	...	2.0	3.0	3.5	4.0	3.1	4.1	2.9
He II 4686	3.0	4.8	4.5	5.0	5.0	5.9	5.4	2.1
Hβ 4861	100.0	100.0	100.0	100.0	100.0	100.0	100.0	100.0
He I 4922	0.5	0.5	...	1.0	1.2	...
[O III] 4959	12.0	...	11.3	11.2	12.0	11.8	25.5	27.8
[O III] 5007	35.0	37.3	37.8	35.9	37.0	35.3	78.3	81.0
He I 5015	2.1	1.8	...	0.9	1.2	...
[N I] 5200	2.0	2.8	1.5	1.4	...	1.4	0.7	6.1
He I 5876	12.0	11.9	14.0	11.0	10.0	10.9	11.2	10.9
[O I] 6300	45.0	68.0	49.7	37.7	34.0	38.2	90.0	119.8
[S III] 6312	0.7	0.6	...	1.0	1.0	...
[O I] 6364	18.4	12.9	9.0	13.3	30.9	38.8
[N II] 6548	10.3	7.0	...	7.1	21.9	...
Hα 6563	417.0	395.0	420.0	300.0	295.0	331.0	301.1	437.9
[N II] 6583	32.0	31.1	27.3	18.3	21.0	20.3	59.2	112.8
He I 6678	3.4	2.4	...	2.8	2.8	4.9
[S II] 6716	60.0	64.5	73.0	50.9	51.0	54.5	85.1	109.3
[S II] 6731	74.0	79.6	96.0	67.0	65.0	71.1	120.6	142.7
He I 7065	5.0	3.3	...	3.7	4.3	3.8
[Ar III] 7136	2.1	1.2	...	1.4	6.3	6.8
[Ca II] 7291	24.0	14.7	24.7	15.9	20.0	19.0	26.9	14.0
[O II] 7319 + [Ca II] 7325	16.0	13.3	25.9	16.6	22.0	17.5	54.1	34.1
[Ni II] 7378	5.6	3.6	...	3.4	9.3	5.4
[Ni II] 7411	0.6	0.4	...	0.6
[Cr II] 8230	3.0	1.8	...	1.7
He II 8237	1.5	0.7	2.5	1.0
[S II] 6716/6731	0.81	0.80	0.76	0.76	0.78	0.77	0.71	0.76
[O III] (4959+5007)/4363	15.4	~10	...	17.4	12.3	14.8	26.6	...
Log I(Hβ) erg cm ⁻² s ⁻¹		-13.19	-13.26		-13.40			

NOTE—Log I(Hβ) values listed are uncorrected for reddening.

References—References – DD83: [Dodorico & Dopita \(1983\)](#); L98: [Lozinskaya et al. \(1998\)](#); Peimbert88: [Peimbert et al. \(1988\)](#); Dopita19: [Dopita et al. \(2019\)](#); RD90: [Russell & Dopita \(1990\)](#)

Table 2. Relative [Fe II] Emission Line Strengths in S8, N49, and N63A

Emission Line (Å)	Multiplet Number	S8			N49		N63A
		this work F(λ)	this work I(λ)	Dopita19 I(λ)	RS90 I(λ)	Vancura92 I(λ)	RS90 I(λ)
[Fe II] 4244, 4245	21F	2.0	2.3	2.6	4.0	...	1.6
[Fe II] 4287	7F	1.2	1.5	2.1	3.6
[Fe II] 4358, 4359	21F, 7F	1.4	1.7	...	13.5
[Fe II] 4414	7F	2.5	2.9	3.1	3.9
[Fe III] 4658	3F	2.0	2.3	1.7	3.9
[Fe III] 4814	3F	1.2	1.4	1.7	2.3	...	2.8
[Fe III] 4882	2F	0.5	0.5	1.0
[Fe II] 4890	4F, 3F	0.6	0.6
[Fe II] 5111	19F	0.5	0.4	0.9	0.8	...	1.6
[Fe II] + [Fe VII] 5159	18F, 19F, 2F	7.7	6.9	6.8	10.2	10.0	5.1
[Fe II] 5220	19F	0.7	0.6	0.6
[Fe II] 5262	19F	3.4	2.7	2.5	4.8	3.5	2.1
[Fe II] 5273	18F	2.6	2.3	0.4	...	1.3	...
[Fe II] 5334	19F	1.2	0.8	0.9	...	1.9	...
[Fe II] 5527	17F	1.6	1.3	1.1	2.0	2.1	...
[Fe II] 7155	14F	12.3	7.8	8.5	16.9	12.6	7.5
[Fe II] 7172	14F	1.9	1.1	1.0	4.1	2.1	...
[Fe II] 7387	14F	2.5	1.8	1.2
[Fe II] 7453	14F	3.6	2.3	2.8	13.9	4.1	9.6
[Fe II] 7638	1F	1.1	0.6	1.1	6.6	1.5	2.6
[Fe II] 7686	14F	1.9	1.0	0.8	2.1	1.5	1.8
[Fe II] 8617	13F	9.2	4.3	9.7	19.9	13.5	12.1
[Fe II] 8892	13F	4.4	1.9	3.1	5.9	4.1	6.0

NOTE—Listed line strengths are relative to $H\beta = 100$.

References—Dopita19: [Dopita et al. \(2019\)](#); RS90: [Russell & Dopita \(1990\)](#); Vancura92: [Vancura et al. \(1992\)](#)

and using atomic level calculations by [De Robertis et al. \(1987\)](#).

From our higher resolution blue grism spectra, we find a 6716/6731 ratio of 0.76 ± 0.013 which suggests an n_e , of 1600 cm^{-3} . However, if we adopt the revised formulation of [Proxauf et al. \(2014\)](#) which used CLOUDY models ([Ferland et al. 2013](#)) to calibrate the density sensitive [S II] 6716/6731 line ratio, this observed ratio translates into a electron density, n_e , of $1060 \pm 100 \text{ cm}^{-3}$. As noted by [Proxauf et al. \(2014\)](#), their model predicts lower densities by some 20% from those of previous works. However, due to the low metallicity of the IC 1613 galaxy, this value must be revised up a bit to $\simeq 1200 \text{ cm}^{-3}$ ([Kewley et al. 2019](#)).

Considering possible differing slit placements by us and previous observers, the agreement for the [S II]

6716/6731 ratio between observers suggests little in the way of density variations across the S8 remnant. However, based on observed differences of the [S II] 6716/6731 ratio across the remnant, [Lozinskaya et al. \(1998\)](#) claim density variations of $400 - 600 \text{ cm}^{-3}$, along with a single dense knot with $n_e \sim 2400 \text{ cm}^{-3}$ along the remnant's northern edge.

The remnant's electron temperature of its O^{+2} emitting regions can be calculated from the ratio, R , equal to $I(4959 + 5007)/I(4363)$ ([Osterbrock & Ferland 2006](#)). If the electron density is $\ll 10^6 \text{ cm}^{-3}$, then $R = 7.90 \times e^{3.29 \times 10^4 / T_e}$. For electron temperatures below $50 \times 10^3 \text{ K}$, the [O III] 4363 Å line is relatively weak relative to the 5007 Å line.

In the case of S8, where the [O III] 4959, 5007 Å lines are not especially strong, estimating an electron tem-

Table 3. Optical Coronal Line Emissions in S8 and Young LMC SNRs

Emission Line (Å)	S8			N49	N63A
	this work	this work	Dopita19	Dopita19	RD90
	F(λ)	I(λ)	I(λ)	I(λ)	I(λ)
[Fe VII] 5720	0.7	0.5	0.3
[Fe VII] 6087	0.9	0.8	1.4	0.4	...
[Fe X] 6374	1.2	0.9	0.5	1.1	...
[Fe XI] 7892	2.1	1.0	1.0	1.8 ^a	0.3
[Fe XIV] 5303	1.1	0.8	1.9	1.2	...

NOTE—Listed line strengths are relative to $H\beta = 100$.

^aN49 line value above 7000 Å is taken from Russell & Dopita (1990).

References—Dopita19: Dopita et al. (2019); RD90: Russell & Dopita (1990)

perature for the O^{+2} based on the much weaker 4363 Å line requires especially good S/N spectra. In addition, as noted by several authors measuring the [O III] electron temperature can be complicated by blending from [Fe II] emissions around 4360 Å with the temperature sensitive [O III] 4363 Å line (Osterbrock & Dufour 1973; Fesen et al. 1982; Peimbert et al. 1988; Curti et al. 2017). Given the numerous [Fe II] lines in the S8 spectrum, blending of [O III] 4363 Å emission with that of [Fe II] emission lines thus poses a concern for obtaining an accurate [O III] electron temperature for the S8 remnant.

Blending of [Fe II] emission with [O III] 4363 Å emission may have lead to artificially small R values in past studies and hence relatively high estimated [O III] temperatures for S8. Dodorico & Dopita (1983) cite a value of 15.4 indicating $T_e \simeq 50 \times 10^3$, while Peimbert et al. (1988) find $R = 12.3$ leading to their estimate of $T_e = (80 \pm 15) \times 10^3$ K. While updated atomic constants would lower this T_e estimate closer to 75×10^3 K, this would still be an exceptionally high temperature for a completely radiative SNR filament (see Fesen et al. 1982; Fesen & Hurford 1996). Lozinskaya et al. (1998) do not list a value for R but their data suggests an even lower value ~ 10 implying $T_e > 10^5$ K. An R value of 14.8 cited by Dopita et al. (2019) implies $T_e \simeq 53,000$ K which is still relatively hot for a radiative shock filament.

Our blue grism spectrum of S8 is of sufficient spectral resolution (3.5 Å) to show a weak blended emission feature around 4361 Å. There are potentially three [Fe II] emission lines which could contribute to a blended feature. Their lab wavelengths and forbidden multiplet numbers are: 4358.10 (6F), 4358.37 (21F), and 4359.34 (7F). Analysis of the observed blended feature suggests just two components near 4359.1 and 4362.6 Å which we attribute to the [Fe II] 4359.34 line and the [O III] 4363.21 line, respectively. This conclusion is supported

by calculated [Fe II] transition probabilities (Garstang 1962), which predicts the 4359.34 (7F) to be stronger than the 4358.37 (21F) line. From deblended extinction corrected intensities relative to $H\beta$, we find the ratio of the [O III] lines $(4959 + 5007)/4363 = 17.4 \pm 1.4$ indicating $T_e = 41,500 \pm 4000$ K for the O^{+2} zone.

3.2.3. Forbidden Iron Emission Lines

The S8 remnant displays a wealth of forbidden Fe lines, both low ionization [Fe II] lines and much higher ionization coronal lines such as [Fe X] and [Fe XIV] (see Fig. 5). Our observed and extinction corrected line strengths of [Fe II] and [Fe III] lines are listed in Table 2, along with extinction corrected values taken from Dopita et al. (2019). As seen in this table, with the exception of lines above 8000 Å, our measurements and those of Dopita et al. (2019) for these forbidden Fe lines are in very good agreement.

Interestingly, the spectrum of S8 also shows the presence of several coronal emission lines of iron (Fig. 4). These include include [Fe X] 6374, [Fe XI] 7892, and [Fe XIV] 5303. Although the [Fe VII] 5720, 6087 are not always included in discussions of iron coronal lines, we include these here since they represent a higher degree of ionization (>99 eV) than the lines listed in Tables 1 and 2.

The detection of optical coronal lines of iron in the spectrum of the S8 was only recently reported (Dopita et al. 2019). Although we were initially unaware of these results when we obtained our spectra, we confirm their basic results except for the issue of [Fe IX] as we discuss below. Coronal line emissions from S8 are somewhat unexpected in view of both the weakness of [O III] emission and the extensive number of [Fe II] lines seen in the spectrum (Table 2) and indicates a wider range of shock velocities present in the remnant than previously realized. Relative line strengths, both observed and extinc-

tion corrected coronal line emissions are shown in Table 3 along with those reported by Dopita et al. (2019).

The presence of [Fe X], [Fe XI], and [Fe XIV] lines, albeit weak, requires postshock plasma temperatures between $1.2\text{--}2.0 \times 10^6$ K (Nussbaumer & Osterbrock 1970). Because the maximum temperature just behind a shock with velocity, V , is approximately

$$T_{\max} \simeq \frac{3}{32} \frac{m_{\text{H}} V^2}{k} \quad (1)$$

postshock temperatures $\sim 2 \times 10^6$ K indicate the presence of shocks with velocities $\simeq 350$ km s $^{-1}$ (see Fig. 5). This estimate is supported by the observed line ratio of the [Fe XIV] 5303/[Fe XI] 7892 of 0.80 (our data) and 0.52 from Dopita et al. (2019) (see Table 3) which suggests a value of ~ 330 km s $^{-1}$ based on computed 5303/7892 line ratios as a function of blast wave velocity (Vogt et al. 2017).

While coronal line emissions are unusual in SNR spectra in general, they have been seen in a few young LMC remnants, namely N49, N63A, and N103b (Dopita & Mathewson 1979; Dopita et al. 2019), and a few especially hot [O III] filaments in the Cygnus Loop which has a blast wave velocity around 350 km s $^{-1}$ (Sauvageot et al. 1990; Fesen & Hurford 1996; Raymond et al. 2015). Keenan & Norrington (1987) showed that the [Fe VII] 5159/6087 line strength ratio is a function of temperature and density, but the 5159 Å emission line is too blended with the [Fe II] lines at 5158 and 5189 to allow an estimate of [Fe VII] gas temperature.

Although we find S8’s coronal line strengths generally in agreement with those reported by Dopita et al. (2019), we do not support their claimed detection of [Fe IX] lines at 4359.1 and 8234.5 Å both in S8 and in some LMC SNRs. If this were true, it would mark the first finding of [Fe IX] line emissions in any SNR (e.g., Fesen & Hurford 1996). Moreover, to our knowledge no [Fe IX] lines have ever been reported detected in AGNs where coronal lines are commonly seen (Nussbaumer & Osterbrock 1970; Ferguson et al. 1997; Nazarova et al. 1999), nor are typically included in general discussions of optical coronal line emissions from hot plasmas (Graney & Sarazin 1990).

Consequently, we view the presence of either of the two [Fe IX] lines cited by Dopita et al. (2019) as unlikely in S8’s spectrum. Weak emission seen at $\simeq 4359$ Å is more plausibly due to a blend of two [Fe II] lines rather than [Fe IX] 4359.1 emission as noted above; namely 4358.37 (21F) and 4359.34 (7F) (Osterbrock & Dufour 1973). Several [Fe II] lines from the 7F multiplets are present in the S8 spectrum (see Table 2), making the identification of the feature near 4359 Å as due to [Fe II] instead of [Fe IX] likely.

Similarly, their identification of [Fe IX] at 8234.5 Å as the weak emission feature around 8234 Å also seems doubtful. In their paper discussing a spectra of the LMC SNRs N49, N63A, and N103b which exhibit spectra sim-

ilar to that of S8, Russell & Dopita (1990) cite only the detection of He II 8236.77 Å around 8230 Å. Moreover, in the spectrum of N49 by Vancura et al. (1992), they cite the presence of [Cr II] 8229.55 Å but list no feature around 8234 Å, where Levenson et al. (1995) find several [Cr II] in this region of N63A’s spectrum. Our spectra show a blended feature with measured centroids at 8221.5 and 8234.2 which we tentatively attribute to a blend of He II 8236.8 and a blend of two [Cr II] lines at 8225.2 and 8229.6 Å.

3.3. High Dispersion Spectra of S8’s H α Emission

Figure 6 shows a 2D image of our moderate resolution spectrum of S8 and neighboring H II regions covering the wavelength region around H α . The small insert image in the left panel shows the location of the long N-S slit on the sky intersecting both S8 and the large emission shell GS4 located to the north (Meaburn et al. 1988). Broad H α and [N II] emissions can be seen associated with the SNR S8, and much narrower emissions from H II regions to both the north and south.

The heliocentric radial velocity of IC 1613 is $V_{\text{HEL}} = -234$ km s $^{-1}$ (Lu et al. 1993)². For the large giant emission shell GS4, Meaburn et al. (1988), found $V_{\text{HEL}} \simeq -230$ km s $^{-1}$ with an expansion velocity of 29 km s $^{-1}$. This expansion velocity is in good agreement with our measured expansion width of 1.31 ± 0.03 Å = 60 ± 2 km s $^{-1}$ for the GS4 shell. In the following discussions, we will adopt GS4’s heliocentric velocity as being the rest velocity for S8’s local environment.

The right panel of Figure 6 shows the remnant’s full detected radial velocities cover a range of ~ 365 km s $^{-1}$, i.e., rest velocities from +120 to -245 km s $^{-1}$, corresponding to $V_{\text{HEL}} = -110$ to -475 km s $^{-1}$. These maximum and minimum heliocentric velocities are in agreement with those of Rosado et al. (2001) and of Lozinskaya et al. (1998), the later who cite $+145 \pm 14$ and -423 ± 13 km s $^{-1}$ which they characterize as ‘high-velocity features’ but which we view as just the velocity extremes of S8’s radial expansion velocities. However, we do not confirm any higher heliocentric velocities in the range of -500 to -800 km s $^{-1}$ as claimed by Lozinskaya et al. (1998).

As shown in the insert image in the right panel of Figure 6, the brighter parts of the remnant H α emission are contained within a fairly small velocity range; i.e., rest frame velocities, $V_{\text{Rest}} = 0$ to -130 km s $^{-1}$. The weight of the remnant’s emission is clearly blueshifted relative to the rest frame of the local H II regions.

The brightest H α emission lies in two broad brightness maxima centered at rest frame velocities of -15 ± 3 and

² Although Sandage is credited with first identifying S8 as an H II region, Sandage notes that M. Humason obtained a radial velocity value for IC 1613 of -238 km s $^{-1}$ (Humason & Wahlquist 1955) based on a spectrum taken of S8 identified as an emission region from a red 200-inch Palomar plate obtained by W. Baade.

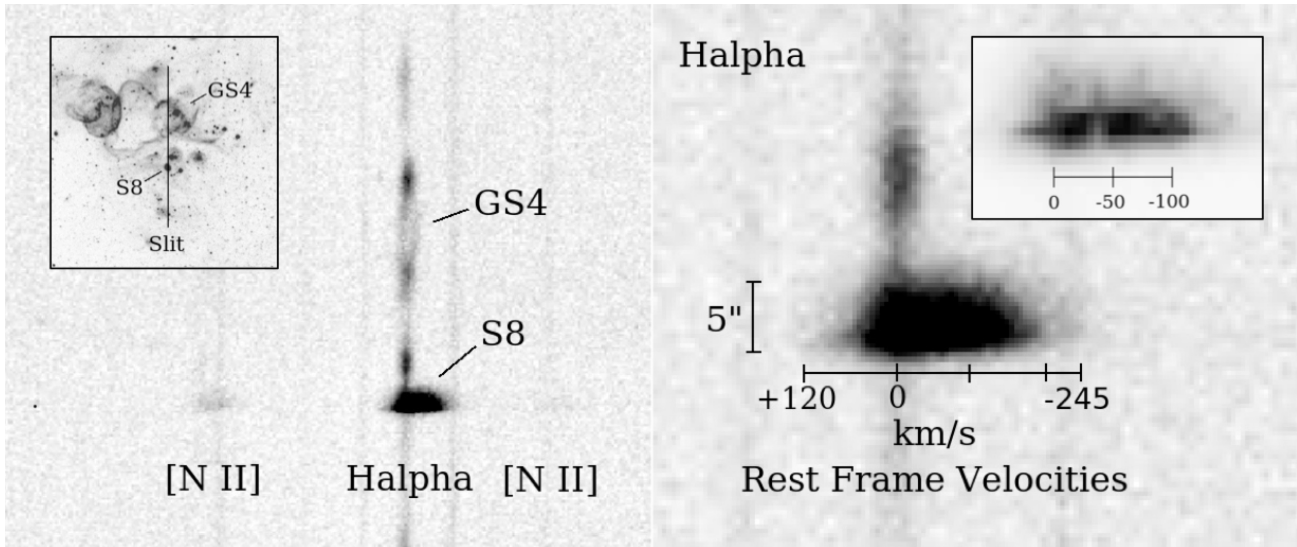


Figure 6. Left panel: 2D moderate resolution spectrum (red to the left, blue to the right) showing $H\alpha$ emissions from S8 and neighboring H II regions. Insert image shows location of the North-South slit crossing over the S8 remnant and the superbubble GS4. North is up, East to the left. The narrow vertical $H\alpha$ emission from the neighboring H II regions was used to establish the rest frame velocity for S8. Right panel: A blow-up of S8’s $H\alpha$ emission showing the remnant’s internal radial velocity structure, its velocity range, and a central cavity. Small insert image shows the 45 km s^{-1} wide emission cavity.

$-65 \pm 5 \text{ km s}^{-1}$ and roughly centered on a cavity-like feature $\sim 37 \text{ km s}^{-1}$. The emission is considerably broader on the more blueside of the $H\alpha$ emission profile extending from -40 to -115 km s^{-1} . Despite their differences in terms of velocity, both the rear and front facing emission maxima exhibit nearly identical peak fluxes.

Both visually and quantitatively, our 2D spectrum presented in Figure 6 agrees largely with the description of S8’s $H\alpha$ emission given by Rosado et al. (2001), that is one consisting of two components, one with a FWHM $= 66 \pm 10 \text{ km s}^{-1}$ centered around a rest velocity of -15 km s^{-1} , with a second and broader component centered around a rest velocity of -100 km s^{-1} . The fact that the facing, blueshifted emission is noticeably more extended than that of the rear redshifted emission suggests the possibility of significant internal extinction between front and rear emission regions, of order $A_{H\alpha} \sim 0.5 \text{ mag}$.

An apparent narrow emission depression or ‘cavity’ between these two bright emission components can also be seen in the right panel’s insert of Figure 6. The emission decrease is relatively small in terms of a change in observed $H\alpha$ emission; flux in between the two emission peaks drops only by about 15% in intensity, rising up to the two brightness peaks within velocity span of just $\sim 20 \text{ km s}^{-1}$. The small decrease in flux of this cavity might be misleading due to our instrumental 24 km s^{-1} resolution. We also note an interesting increase of emission northward along the slit exactly coincident with the cavity’s central velocity.

The reality of this emission cavity is confirmed on the three individual spectra obtained. It is also supported by the above described findings of Rosado et al. (2001) and by a similar expansion cavity reported by

Lozinskaya & Podorvanyuk (2009) who find a $75 \pm 25 \text{ km s}^{-1}$ velocity between front and rear hemispheres. This is larger than the $\simeq 45 \text{ km s}^{-1}$ we find. However, this difference may simply reflect that our spectral slit was not placed in the largest expansion area of the remnant. Also as noted above, the more blueshifted maximum emission peak is a broader than the red peak. If measured from the velocity average of the broader blueshifted emission rather than its peak, our data would imply a somewhat larger expansion cavity $\sim 55 \text{ km s}^{-1}$.

The remnant’s expansion velocity as measured from the $H\alpha$ emission profile (Fig. 6) suggests a value around 180 km s^{-1} . However, if measured from the rest velocity of the $H\alpha$ emission cavity, then the maximum blueshifted velocity we detected is closer to $\simeq 200 \text{ km s}^{-1}$ (see Fig. 6).

Finally, these spectra indicate that the remnant’s $H\alpha$ emission with $V_{\text{rest}} \simeq +50$ to -150 km s^{-1} is present across 4-5 arcsec along the N-S slit, with faint extensions farther northward with rest frame radial velocities of -60 to -85 , -110 , and -135 km s^{-1} . We speculate that one of these might be associated with the narrow filament along the remnant’s northern limb seen in the direct $H\alpha$ image (Fig. 3, right panel).

4. DISCUSSION

The bright SNR S8 in the dwarf galaxy IC 1613 has been the subject of nearly a dozen investigations since its first identification by Sandage in 1971. These studies have led to a variety of descriptions of the S8 nebula and conclusions about its nature. Below we discuss its basic physical parameters derived from both our new

findings and earlier observations, compare S8 to other young SNRs, and then state our conclusions about its nature.

4.1. S8's Physical Properties

4.1.1. Shock Velocity and Electron Density

The remnant's expansion velocity as measured from our observed H α emission profile suggested a maximum velocity around 180 km s⁻¹. Comparisons of its spectral line ratios with a variety shock models suggest shock velocities a bit lower, around 100 - 150 km s⁻¹ (Peimbert et al. 1988; Lozinskaya et al. 1998).

In contrast, Dopita et al. (2019) claimed to only find good agreement of S8's observed spectra using shock models having two very different shock velocities; a fairly slow one ~ 50 km s⁻¹ plus a much faster one ~ 230 km s⁻¹ in a ratio of 2:3. While such a mixed velocity model predicted overly strong He II and [O III] line emissions compared to observations, it did match the observed [Fe VII] line strength.

A range of shock velocities would be consistent with the presence numerous [Fe II] emission lines and the presence of [O III] line emission which requires a minimum shock velocity ~ 100 km s⁻¹ (Raymond 1979). Analysis of S8's optical spectra by Peimbert et al. (1988) suggested shock velocities as high as 160 km s⁻¹ to explain S8's optical spectrum, whereas Rosado et al. (2001) suggested an even higher value V_s of 170 km s⁻¹.

However, the presence of high ionization coronal lines, especially that of [Fe XIV], indicates much higher shock velocities at least ~ 350 km s⁻¹ (Dopita & Mathewson 1979). The ratio of the strength of the [Fe X] 6374 relative to [Fe XIV] 5303 around 1 (Table 3) suggests a electron temperature around 1.6×10^6 K under the assumption of a single temperature cause by collisional ionization and excitation (Nussbaumer & Osterbrock 1970) which requires a velocity ~ 400 km s⁻¹.

The simultaneous presence of dozens of low ionization emission lines together with all the commonly reported optical coronal lines typically observed in gas at temperatures $1 - 3 \times 10^6$ K clearly signals a wide range of shock velocities likely generated by large variations in preshock gas densities like that of a multi-phase ISM cloud-intercloud arrangement. Exactly such a scenario has been proposed in several other SNRs and actually for S8 by Lozinskaya & Podorvanyuk (2009) who, not knowing about S8's coronal line emissions, based this conclusion on the remnant's X-ray luminosity.

As discussed above, the electron density of the remnant's emission filaments from the [S II] 6716/6731 line ratio indicates $n_e = 1000 - 1600$ cm⁻³. From this we can estimate the preshock density from the equation

$$N_{[S II]} \simeq 31 - 45 (V_s/100 \text{ km s}^{-1})^2 (n_o/\text{cm}^{-3}) \quad (2)$$

where n_o is the preshock electron density and V_s is the shock velocity responsible for the [S II] emission (Dopita 1979; Russell & Dopita 1990; Rosado et al. 2001).

Taking $N_{[S II]} = \sim 1400$ and adopting a shock velocity range of 120 - 150 km s⁻¹, we find $n_o \sim 10 - 30$ cm⁻³. A similar preshock density range was found by Peimbert et al. (1988), Lozinskaya et al. (1998), and Rosado et al. (2001).

4.1.2. Mass

We can estimate the emitting mass of S8 using the observed H α flux. Our extinction corrected H β flux measurement of 1.3×10^{-13} erg cm⁻² s⁻¹ using a long N-S 1.4'' wide slit corresponds to a total S8 H α flux value of $\simeq 6 \pm 1.5 \times 10^{-13}$ erg cm⁻² s⁻¹. Adopting this extinction corrected value, an electron density $N_e = 1400 \pm 200$ cm⁻³, and a distance to IC 1613 of 725 kpc, we estimate the mass of ionized hydrogen, $M_{H^+} = 85 \pm 24 M_\odot$ using

$$M_{H^+} = \frac{m_p 4\pi d^2 F^c(\text{H}\alpha)}{h\nu_{\text{H}\alpha} \alpha_{\text{H}\alpha}^{eff}(H^0, T_e) N_e} \quad (3)$$

where m_p is the mass of the proton, $F^c(\text{H}\alpha)$ is the extinction corrected H α flux, $h\nu_{\text{H}\alpha}$ is the energy of an H α photon, and $\alpha_{\text{H}\alpha}^{eff}(H^0, T_e)$ is the effective recombination coefficient of H α equal to 8.7×10^{-14} erg cm⁻² s⁻¹ for 10^4 K (Osterbrock & Ferland 2006). Assuming an abundance ratio of H:He of 10:1 by number, this leads to a total mass estimate of $119 \pm 34 M_\odot$. This is an order of magnitude less than the 1900 M_\odot estimated by (Peimbert et al. 1988) of swept of material but much more than the 15 M_\odot they estimated for a thin emitting shell.

The emitting mass of S8 likely consists of both swept-up local ISM material and any pre-SN mass loss from the progenitor. Assuming a ellipsoid shell dimensions of 6 pc x 6 pc x 9 pc, consistent with S8's projected angular size of 3''.5 x 5''.0, and a local H I ISM density $\sim 1 - 3$ cm⁻³ (Lozinskaya et al. 2001), the remnant could have swept up 35 - 105 M_\odot . The upper mass range of this estimate is consistent with the notable increased H I 21 cm emission in maps of the region around the S8 remnant (Lozinskaya 2002; Lozinskaya & Podorvanyuk 2009).

4.1.3. Age and SN Energy

Assuming the S8 remnant is in an adiabatic expansion phase, we can use the Sedov expression

$$E_o = 1.37 \times 10^{42} n_o V_s^2 R_s^3 \quad (4)$$

to estimate the energy of the S8 SN explosion where E_o is the SN energy in ergs, n_o is the preshock density per cm⁻³ associated with the estimated shock velocity, V_s in km s⁻¹ and the shock radius, R_s in pc. Adopting $V_s = 180$ km s⁻¹ based on the remnant's strong blueshifted H α velocity measured from the central cavity, $n_o \sim 20$ cm⁻³ associated with S8's H α emission as discussed above, and an average radius $R_s = 7.5$ pc, then $E_o \sim 4 \times 10^{50}$ erg.

We can also estimate the age of the S8 remnant using the Sedov expression which relates age to radius and blast wave by the expansion timescale equation

$$t = 0.4 \times (\text{radius}/V_{\text{blast}}). \quad (5)$$

Taking S8's average angular diameter of $\simeq 4''.25$ which translates to a radius of 7.5 pc at 725 kpc, and assuming a minimum blast wave velocity of 350 km s^{-1} based on the presence of [Fe XIV] emission, gives a maximum age of $\sim 8400 \text{ yr}$. However, X-ray observations suggest a much faster blast wave velocity of $660 - 1100 \text{ km s}^{-1}$ (Schlegel et al. 2019) which would imply an age of just $\sim 2700 - 4400 \text{ yr}$.

One can check this estimated age range by using the estimated SN energy calculated above in the Sedov expression for remnant radius,

$$r = 1.54 \times 10^{19} \text{ cm } E_{51}^{1/5} n_0^{-1/5} t_{1000\text{yr}}^{-3/5} \quad (6)$$

where E_{51} is SN energy in units of 10^{51} erg , n_0 is the density in cm^{-3} , and $t_{1000\text{yr}}$ is the SNR age in units of 1000 yr. Assuming an age of 3500 yr, a SN energy of $0.4 \times 10^{51} \text{ erg}$ and a density $\sim 1 \text{ cm}^{-3}$ consistent with H I measurements around S8, we find a remnant radius, $r = 6.8 \text{ pc}$ consistent with the remnant's average radius of 7.5 pc and observed dimensions of $12 \times 18 \text{ pc}$.

4.2. The Nature of the S8 Supernova Remnant

Following Sandage's initial identification of S8 as an H II region, it was classified as a SNR based on optical spectra showing the characteristically strong [S II] emission relative to $\text{H}\alpha$ of shocked gas seen in SNRs (Smith 1975; Dodorico & Dopita 1983; Peimbert et al. 1988) plus the detection of a nonthermal radio spectrum Dickel et al. (1985). However, a simple SNR classification was challenged when Armandroff & Massey (1985) claimed a Wolf-Rayet (WR) star was present along its northeastern limb based on flux measurements in narrow passband filters centered around He II 4686 Å. A follow-up study by Massey et al. (1987) found its spectrum 'quite peculiar' and suggested the supernova remnant likely contained a Wolf-Rayet (W-R) star based on the presence of broad He II line emission arising from a point-like source with strong continuum emission.

Subsequent spectra by Armandroff & Massey (1991), however, found no unusual broadening of its He II line emission leading them to discount their previous assessment that S8 harbored a W-R star. They concluded S8 was likely a young SNR, but noted its spectrum was unlike that of any SNR in M31 and M33. They also pointed out the presence of continuum emission plus He II and [Fe II] emissions resembled those seen in the Crab Nebula, while also noting that other young SNRs exhibit strong He II and [Fe II] emissions such as the LMC remnants N49, and N63A.

While Peimbert et al. (1988) estimated S8 was a fairly evolved SNR with an age $\sim 20,000 \text{ yr}$, later studies concluded it was relatively young. Lozinskaya et al. (1998)

estimated S8's age as $\sim 3000 - 6000 \text{ yr}$. They also suggested it was created by a supernova explosion inside an H I shell and compared it to the young LMC remnant N49.

Rosado et al. (2001) and Schlegel et al. (2019) suggested instead it resembled more the LMC remnant N63A. While Dopita et al. (2019) found S8's spectral similarities to both N49 and N63A, both Armandroff & Massey (1991) and Schlegel et al. (2019) discussed S8 as a possible 'plerion' type of remnant like the Crab Nebula. Recently, Schlegel et al. (2019) concluded it was likely a mixed morphology or composite type remnant containing both a outer thermal emission shell enclosing nonthermal emission like that of a pulsar wind nebula.

One similarity of S8 to the Crab Nebula is that both exhibit significant continuum emission, which in the case of the Crab is due to a bright pulsar wind nebula off its powerful central 33 ms pulsar. Schlegel et al. (2019) noted that S8's filled X-ray emission structure in resolved *Chandra* images are suggestive of a Crab-like plerion or composite SNR. However, besides obvious differences in age and expansion velocities, S8's optical spectrum is unlike that of the Crab Nebula, in particular it lacks the Crab's unusually strong nitrogen and helium lines (Davidson 1973; Fesen & Kirshner 1982; MacAlpine & Uomoto 1991; MacAlpine & Satterfield 2008; Satterfield et al. 2012; Sibley et al. 2016).

On the other hand, as shown in Tables 1 to 3, S8's optical spectrum is remarkably similar to that of two young core-collapse SNRs in the LMC, namely N49 and N63A. Considering IC 1613's even lower metallicity than the LMC leading to weaker oxygen, nitrogen and sulfur emission lines, S8 exhibits an optical spectrum especially close to that observed for these young LMC remnants.

However, whereas Rosado et al. (2001) and Schlegel et al. (2019) suggest S8 is more like N63A than N49, we find N49 to be the better match to the S8 remnant. Both have similar [S II], [N II], and [O III] line strengths relative to $\text{H}\alpha$, nearly identical electron density sensitive [S II] line ratios, similar [O III] electron temperatures, relative strengths of [Fe II] emission lines and coronal Fe emissions.

In addition, besides exhibiting strikingly similar optical spectra, S8 and N49 are of similar size, estimated age and mass, shock velocities, and optical and X-ray luminosities as shown in Table 4. Although the N49 remnant is known for possessing the Soft Gamma-Ray Repeater, SGR 0526-66, no compact object has been identified in S8 based on its optical or X-ray observations (Schlegel et al. 2019).

Finally, there is the puzzle concerning S8's strong optical continuum emission, clearly seen in Figures 2 and 3 and it was this that initially led to speculations about a continuum point source(s) present within the remnant. SNRs exhibiting any appreciable continuum are exceedingly rare, with the Crab Nebula being the most famous case. It was the presence of S8's continuum emission

Table 4. Comparison of S8 with LMC Remnants N49 and N63A

Property	S8	N49	N63A	S8 Refs ^a	N49 Refs ^b	N63A Refs ^c
Physical Dimensions	12 pc × 18 pc	16 – 18 pc	16 pc	1, 2, 3	1	1
Estimated Age	2700 – 4400 yr	3000 – 5400 yr	2000 – 5000	1, 4, 5	1, 2	1, 2
Estimated Nebula Mass	119 ± 34 M _⊙	207 ± 66 M _⊙	< 450 M _⊙	1	3	1
Expansion Velocities	+120; –245 km s ^{−1}	+150; –220 km s ^{−1}	+65; –245 km s ^{−1}	1, 4, 6, 7	4	3
Shock Velocities	50 – 230 km s ^{−1}	50 – 270 km s ^{−1}	100 – 125 km s ^{−1}	1, 4, 7, 8, 9	5, 6, 7	4, 5
Blast Wave Velocity	600 – 1100 km s ^{−1}	~ 730 km s ^{−1}	> 350 km s ^{−1}	4, 5	1	6, 7
Filament Density	1400 ± 200 cm ^{−3}	500 – 3500 cm ^{−3}	900 – 1400 cm ^{−3}	1, 4, 6, 8	1, 3, 5, 7	6, 8
Preshock Density	10 – 30 cm ^{−3}	20 – 940 cm ^{−3}	30 – 100 cm ^{−3}	1, 4, 6, 8	1	4, 6
Coronal Line Emissions	[Fe VII] to [Fe XIV]	[Fe VI] to [Fe XIV]	[Fe XI], [Fe XIV]	1, 9	5, 8, 9	9, 10
[Fe XIV] 5303/Hβ	0.8	1.2	0.9 – 3.0	1, 9	5	9
[Fe XI] 7892/Hβ	1.0	1.8	0.3	1, 9	5	10
He I 5876/Hβ	11	11	11	1, 4, 8, 9	1, 10	8, 9, 10
He II 4686/Hβ	5	5	2	1, 4, 8, 9	5, 10, 11	8, 9, 10
Hα Luminosity	3.8 × 10 ³⁷ erg s ^{−1}	2.9 × 10 ³⁷ erg s ^{−1}	2.1 × 10 ³⁵ erg s ^{−1}	1	1	8, 9
X-ray Luminosity	5.6 × 10 ³⁶ erg s ^{−1}	6.4 × 10 ³⁶ erg s ^{−1}	1.9 × 10 ³⁷ erg s ^{−1}	5	12	11
Radio Spectral Index, α	−0.57 ± 0.054	−0.58 ± 0.04	−0.74 ± 0.2	4	13	12

^aS8 References: 1) this paper; 2) Sandage (1971); 3) Dodorico et al. (1980); 4) Lozinskaya et al. (1998); 5) Schlegel et al. (2019); 6) Rosado et al. (2001); 7) Lozinskaya & Podorvanyuk (2009), 8) Peimbert et al. (1988); 9) Dopita et al. (2019).

^bN49 References: 1) Vancura et al. (1992); 2) Park et al. (2012); 3) Melnik & Copetti (2013); 4) Chu & Kennicutt (1988); 5) Dopita et al. (2019); 6) Dennefeld (1986); 7) Pauletti & Copetti (2016); 8) Murdin et al. (1978); 9) Dopita & Mathewson (1979); 10) Russell & Dopita (1990); 11) Dopita et al. (2016); 12) Maggi et al. (2016); 13) Dickel & Milne (1998).

^cN63A References: 1) Warren et al. (2003); 2) Hughes et al. (1998); 3) Chu & Kennicutt (1988); 4) Dopita (1979); 5) Lasker (1981); 6) Shull (1983); 7) Rosado (1986); 8) Levenson et al. (1995); 9) Dopita & Mathewson (1979); 10) Russell & Dopita (1990); 11) Maggi et al. (2016) 12) Bozzetto et al. (2017).

that caused Massey et al. (1987) to propose that S8 might be a Crab-like remnant.

In view of the strength of S8’s continuum emission, it is somewhat surprisingly that only Massey and collaborators emphasized the unusual finding of strong continuum emission in S8, a property absent in the vast majority of SNRs. Although Lozinskaya et al. (1998) noted that some continuum emission was indeed present in S8, they called for additional observations to determine its extent and intensity and did not discuss possible origins except to say that it could be consistent with a faint superimposed star in the south-central portion of the remnant. It is also surprisingly that neither Peimbert et al. (1988) nor Dopita et al. (2019) make any mention of the presence of coincident continuum emission despite it being obvious in even much lower quality spectra (e.g., Massey et al. 1987).

The solution to S8’s puzzling continuum emission lies in N49’s optical properties. Using a 6100 Å continuum filter (FWHM = 130 Å) much like our continuum 6071 Å filter (FWHM = 260 Å) which avoids any strong emis-

sion lines, Vancura et al. (1992) found N49 to have a surprising amount of continuum emission plus a filamentary morphology nearly identical to that seen in the remnant’s Hα emission. From their Hα and 6100 Å images, they estimated a reddening corrected continuum flux ≃ 4% that of Hα. This flux was within 20% of their estimated H and He recombination continuum along with a minor contribution from two photon continua.

We find S8’s continuum emission in our 6071 filter to also be ≃4% of that of Hα emission. However, considering our 6071 filter’s wider bandpass, this is only about half that seen in N49. Despite this, the fact that S8’s continuum emission closely matches the size and morphology to that seen in Hα, like that seen in N49, argues that S8’s continuum emission is also due to H and He recombination continuum.

S8’s continuum emission may be stronger at shorter wavelengths based on its appearance in the Sloan u band image, where its morphology does not seem as concentrated toward the remnant’s southwestern limb as in the other images and where the remnant is brightest in Hα.

Table 5. Possible Extragalactic SNRs Like S8

Property	M33	NGC 300
Remnant ID	L10-039	S26
Physical Dimensions	16 pc	13 × 15 pc
Estimated Age	...	3300 ± 700 yr
Expansion Velocities	440 km s ⁻¹	~ 400 km s ⁻¹
[S II] 6716/6731	0.75	0.92
Filament Density	1600 cm ⁻³	≈ 1000 cm ⁻³
Coronal Line Emissions	[Fe XIV]	...
Observed H α Luminosity	9.6 × 10 ³⁶ erg s ⁻¹	1.2 × 10 ³⁷ erg s ⁻¹
X-ray Luminosity	3.1 × 10 ³⁶ erg s ⁻¹	1.5 × 10 ³⁷ erg s ⁻¹

References—M33: Long et al. (2010), Long et al. (2018), Blair et al. (1988); NGC 300: Blair & Long (1997), Millar et al. (2011), Read & Pietsch (2001), Gross et al. (2019)

If true, this raises the possibility of a pulsar wind nebula inside the remnant displaced farther to the east. Such an eastern displacement is in the direction where Schlegel et al. (2019) noted evidence, albeit weak, for a possible point source in *Chandra* X-ray images of the S8 remnant.

4.3. Are There Other Extragalactic SNRs Like S8?

The finding that S8 is a young “N49-like” SNR raises the question how unusual are these young and luminous remnants, and might there other similar extragalactic SNRs already detected but not identified as such? Currently, there are over 1500 extragalactic SNRs detected in a dozen or so nearby galaxies (Long 2017, 2019). A key element that sets S8 and N49 apart from most other extragalactic SNRs is their relative youth meaning they still possess high blast wave velocities ($\sim 500 - 1000$ km s⁻¹). If these remnants expand into an extensive multiphase ISM cloud, this will lead to a range of shock velocities, high filament densities $> 10^{3-4}$ cm⁻³, high optical and X-ray luminosities, H and He recombination continuum, and coronal line emissions from lower density regions.

More than two dozen optical extragalactic SNR searches have shown that the majority of remnants are old and large with diameters greater than 20 pc. Few remnants show a density sensitive [S II] 6716/6731 line ratio below unity, indicative of $n_e \geq 1000$ cm⁻³ (Long et al. 2010; Leonidaki et al. 2013; Blair et al. 2014b; Long et al. 2018). This suggests that N49-like remnants might be identifiable using the criteria of a small physical size (dia. ≤ 20 pc) plus [S II] 6716/6731 ratios < 1 . In addition, if such remnants had fast shocks impacting dense CSM or ISM clouds, they would also exhibit high optical and X-ray luminosities like seen for S8 and N49.

A non-exhaustive review of extragalactic SNR surveys reveals a few potential S8 and N49 like remnants (see

Table 5). For example, out of 197 M33 SNRs identified (Long et al. 2010, 2018), the remnant L10-039 (DDB-7, Dodorico et al. 1980) shows the highest H α surface brightest, the largest H α flux, the greatest H α velocity width (FWHM = 443 km s⁻¹; Blair et al. 1988) and is one of only two remnants with a 6716/6731 ratio < 1.0 . Moreover, a plot of its optical spectrum shown in Long et al. (2018, their Fig. 2) appears to show the presence of [Fe XIV] 5303 Å emission which would support a shock velocity above 350 km s⁻¹.

The S26 remnant in NGC 300 also shows some S8-like properties. It is optically the brightest SNR in this spiral galaxy and the only one with a [S II] derived density of ~ 1000 cm⁻³ (Blair & Long 1997). It is also one of the smallest SNRs in the galaxy (dia. $\simeq 15$ pc), appears relatively young with an estimated age ~ 3300 yr and a shock velocity ~ 450 km s⁻¹ based on its X-ray properties (Gross et al. 2019).

4.4. The Missing SN Ejecta in Young Remnants

Lastly, neither of the suspected core-collapse remnants, S8 and N49, show any signs of emissions from high-velocity metal-rich ejecta as one might expect due to their relatively young ages (≤ 5000 yr). This is in contrast to high-velocity, O-rich ejecta knots and filaments present in some other similarly young remnants.

For example, the 3700 – 4500 yr old Galactic remnant Puppis A shows several 1500 km s⁻¹ O-rich ejecta knots and filaments. The much younger 1000 – 2000 yr old SMC remnant 1E0102-7219 consists almost entirely of O-rich ejecta expanding at -2500 to $+3500$ km s⁻¹ (Tuohy & Dopita 1983; Finkelstein et al. 2006; Vogt & Dopita 2010), roughly half that of the younger 350 yr old Galactic SNR, Cassiopeia A.

In an *HST* search of young SNRs in M83, none of the 50+ smallest and presumably young remnants (dia. < 15 pc) showed any optical emissions indicating the pres-

ence of O-rich ejecta, leading Blair et al. (2014a,b) to wonder about the cause of the missing ejecta-dominated remnants in such small remnants. Follow-up Gemini-S GMOS spectra confirmed the lack of obvious ejecta-enhanced abundances and revealed no high expansion velocities. Their sample of small remnants included ones as small as Cas A (dia. = 5 pc) but exhibited only narrow, low-velocity line emissions indicative of ordinary radiative ISM shocks. A few objects such as B12-150 exhibited a [S II] 6716/6731 ratio of 0.75 indicating an electron density around 1600 cm^{-3} , much like S8 and N49 which might have suggested a young age. But no high-velocity emissions were detected.

In light of these findings, objects like S8 and N49 may represent a later evolutionary phase of younger remnants like the small SNRs seen in M83 which lack of optical emission from high-velocity ejecta. For there to be detectable late-time ejecta emission, there must be enough dense ejecta clumps to be readily visible, plus a significant source of excitation and ionization. Possible sources include strong reverse-shock heating, high-velocity interaction with surrounding CSM or ISM, and X-ray and UV emissions from a pulsar-wind nebula.

Regardless of the energy source, whether or not SN ejecta are optically bright is determined by the object's emitting column density and whether the electron density and temperature of the gas are within a certain range of values ($n_e \geq 10 \text{ cm}^{-3}$, $T_e \sim 10^4 - 10^5 \text{ K}$). We speculate that the underlying cause for the lack of optically detectable ejecta in some 2500 – 5000 yr old SNRs may be that only a small fraction of the remnant's mass of high-velocity, O-rich ejecta are presently dense enough and at the right temperature to be visible optically. It may be that in many thousand year old remnants the density of the majority of their ejecta clumps and filaments are below detection limits due to knot disruption after passage of the reverse shock and by knot ablation and fragmentation, like that seen in Cas A's ejecta knots (Fesen et al. 2011), during the centuries long interaction phase with the local ISM.

5. CONCLUSIONS

In this paper we have presented high resolution optical images and spectra of the compact SNR, S8, in the nearby dwarf galaxy IC 1613. $H\alpha$ images of the remnant show a sharply defined crescent shaped nebula $3''.5 \times 5''.0$ in size which is 12 pc x 18 pc at IC 1613's distance of 725 kpc. Narrow passband images clear of the remnant's bright emission lines reveal a coincident and unexpectedly bright continuum nebulosity exhibiting a size and morphology like that seen for the remnant's line emissions.

Low-dispersion spectra reveal numerous low-ionization line emissions such as [O I] and [Fe II], along with higher-ionization emission lines including He II and optical coronal lines ([Fe VII], [Fe X], [Fe XI], and [Fe XIV]) indicating a wide range of shock velocities

present, from ~ 50 to over 350 km s^{-1} , due to multi-phase ISM with preshock densities of $\sim 1 - 30 \text{ cm}^{-3}$. Higher resolution optical spectra indicate an expansion velocity around 180 km s^{-1} with a central cavity $\simeq 45 \text{ km s}^{-1}$ wide. From reddened correct $H\alpha$ flux, we estimate a total nebula mass of $119 \pm 34 M_\odot$ and a remnant age of $\simeq 2700 - 4400 \text{ yr}$.

Combining past research plus our new data, we conclude the S8 supernova remnant is remarkably like those seen in the similarly young LMC remnant N49 including physical size, shock and expansion velocities, filament densities, optical line strengths, X-ray and optical luminosities, along with optical coronal lines and continuum emissions. Both remnants are relatively young possessing a high velocity blast wave ($600 - 1500 \text{ km s}^{-1}$) which has interacted with dense interstellar clouds; in the case of N49 molecular clouds, and H I clouds for S8.

Further study of the S8 remnant could include much higher spatial resolution optical imaging using *HST* to investigate the remnant's line emission structure in comparison with N49's extensive and thin filamentary appearance. Deep narrow passband, line emission-free images could also explore the remnant's continuum emission structure in relation to that seen in its line emission, and investigate continuum emission coincident with a possible point X-ray source hinted at in *Chandra* images.

Because of S8's unusual properties, it would also be of interest to search and identify other similar young SNRs. Follow-up optical spectra of the remnants L10-039 in M33, S26 in NGC 300 and other similar objects could explore their nature through spectral line modeling, expansion velocity measurements, and the possible detection of high-velocity ejecta. Assembling a larger set of young 2500 – 5000 yr old SNRs would lead to a better understanding of the general properties of remnants during their early phases of expansion and evolution.

ACKNOWLEDGMENTS

We thank the referee for helpful comments and suggestions, and Justin Rupert and Eric Galayda and the MDM staff for outstanding assistance that made these observations possible. We also thank Taniiana Lozinskays, Roger Chevalier, Dan Milisavljevic, and Mike Beitenholz for helpful comments. K.E.W. acknowledges support from Dartmouth's Guarini School of Graduate and Advanced Studies, and the Chandra X-ray Center under CXC grant GO7-18050X. This work is part of R.A.F.'s Archangel III Research Program at Dartmouth. Finally, we would like to acknowledge Mike Dopita not only for his research on S8 and young LMC SNRs but his enormous legacy spanning more than four decades on the study and spectral modeling of supernova remnants and other emission line nebulae.

Facilities: Hiltner (OSMOS), McGraw (CCDS)

Software: PYRAF (Green 2012), Astropy v4.0 (Astropy Collaboration et al. 2013, 2018), ds9 (Smithsonian Astrophysical Observatory 2000), L.A. Cosmic (van

Dokkum 2001), OSMOS Pipeline (thorosmos: <https://github.com/jrthorstensen/thorosmos>)

REFERENCES

- Armandroff, T. E., & Massey, P. 1985, *ApJ*, 291, 685, doi: [10.1086/163107](https://doi.org/10.1086/163107)
- . 1991, *AJ*, 102, 927, doi: [10.1086/115924](https://doi.org/10.1086/115924)
- Astropy Collaboration, Robitaille, T. P., Tollerud, E. J., et al. 2013, *A&A*, 558, A33, doi: [10.1051/0004-6361/201322068](https://doi.org/10.1051/0004-6361/201322068)
- Astropy Collaboration, Price-Whelan, A. M., Sipőcz, B. M., et al. 2018, *AJ*, 156, 123, doi: [10.3847/1538-3881/aabc4f](https://doi.org/10.3847/1538-3881/aabc4f)
- Berger, T. A., Kudritzki, R.-P., Urbaneja, M. A., et al. 2018, *ApJ*, 860, 130, doi: [10.3847/1538-4357/aac493](https://doi.org/10.3847/1538-4357/aac493)
- Blair, W. P., Chu, Y. H., & Kennicutt, R. C. 1988, in *IAU Colloq. 101: Supernova Remnants and the Interstellar Medium*, ed. R. S. Roger & T. L. Landecker, 193
- Blair, W. P., Dopita, M. A., Ghavamian, P., et al. 2014a, in *American Astronomical Society Meeting Abstracts*, Vol. 223, American Astronomical Society Meeting Abstracts #223, 453.14
- Blair, W. P., & Long, K. S. 1997, *ApJS*, 108, 261, doi: [10.1086/312958](https://doi.org/10.1086/312958)
- Blair, W. P., Chandar, R., Dopita, M. A., et al. 2014b, *ApJ*, 788, 55, doi: [10.1088/0004-637X/788/1/55](https://doi.org/10.1088/0004-637X/788/1/55)
- Bozzetto, L. M., Filipović, M. D., Vukotić, B., et al. 2017, *ApJS*, 230, 2, doi: [10.3847/1538-4365/aa653c](https://doi.org/10.3847/1538-4365/aa653c)
- Branch, D., & Wheeler, J. C. 2017, *Supernova Explosions* (Springer), doi: [10.1007/978-3-662-55054-0](https://doi.org/10.1007/978-3-662-55054-0)
- Chevalier, R. A. 2005, *ApJ*, 619, 839, doi: [10.1086/426584](https://doi.org/10.1086/426584)
- Chu, Y.-H., & Kennicutt, Robert C., J. 1988, *AJ*, 95, 1111, doi: [10.1086/114706](https://doi.org/10.1086/114706)
- Curti, M., Cresci, G., Mannucci, F., et al. 2017, *MNRAS*, 465, 1384, doi: [10.1093/mnras/stw2766](https://doi.org/10.1093/mnras/stw2766)
- Davidson, K. 1973, *ApJ*, 186, 223, doi: [10.1086/152492](https://doi.org/10.1086/152492)
- De Robertis, M. M., Dufour, R. J., & Hunt, R. W. 1987, *JRASC*, 81, 195
- Dennefeld, M. 1986, *A&A*, 157, 267
- Dickel, J. R., Dodorico, S., & Silverman, A. 1985, *AJ*, 90, 414, doi: [10.1086/113747](https://doi.org/10.1086/113747)
- Dickel, J. R., & Milne, D. K. 1998, *AJ*, 115, 1057, doi: [10.1086/300246](https://doi.org/10.1086/300246)
- Dodorico, S., & Dopita, M. 1983, in *IAU Symposium*, Vol. 101, *Supernova Remnants and their X-ray Emission*, ed. J. Danziger & P. Gorenstein, 517–524
- Dodorico, S., Dopita, M. A., & Benvenuti, P. 1980, *A&AS*, 40, 67
- Dopita, M. A. 1979, *ApJS*, 40, 455, doi: [10.1086/190594](https://doi.org/10.1086/190594)
- Dopita, M. A., & Mathewson, D. S. 1979, *ApJL*, 231, L147, doi: [10.1086/183022](https://doi.org/10.1086/183022)
- Dopita, M. A., Seitzzahl, I. R., Sutherland, R. S., et al. 2019, *AJ*, 157, 50, doi: [10.3847/1538-3881/aaf235](https://doi.org/10.3847/1538-3881/aaf235)
- . 2016, *ApJ*, 826, 150, doi: [10.3847/0004-637X/826/2/150](https://doi.org/10.3847/0004-637X/826/2/150)
- Ferguson, J. W., Korista, K. T., & Ferland, G. J. 1997, *ApJS*, 110, 287, doi: [10.1086/312998](https://doi.org/10.1086/312998)
- Ferland, G. J., Porter, R. L., van Hoof, P. A. M., et al. 2013, *RMxAA*, 49, 137. <https://arxiv.org/abs/1302.4485>
- Fesen, R. A., Blair, W. P., & Kirshner, R. P. 1982, *ApJ*, 262, 171, doi: [10.1086/160408](https://doi.org/10.1086/160408)
- Fesen, R. A., & Hurford, A. P. 1996, *ApJS*, 106, 563, doi: [10.1086/192348](https://doi.org/10.1086/192348)
- Fesen, R. A., & Kirshner, R. P. 1982, *ApJ*, 258, 1, doi: [10.1086/160043](https://doi.org/10.1086/160043)
- Fesen, R. A., Zastrow, J. A., Hammell, M. C., Shull, J. M., & Silvia, D. W. 2011, *ApJ*, 736, 109, doi: [10.1088/0004-637X/736/2/109](https://doi.org/10.1088/0004-637X/736/2/109)
- Finkelstein, S. L., Morse, J. A., Green, J. C., et al. 2006, *ApJ*, 641, 919, doi: [10.1086/500570](https://doi.org/10.1086/500570)
- Garcia, M., Herrero, A., Najarro, F., Lennon, D. J., & Alejandro Urbaneja, M. 2014, *ApJ*, 788, 64, doi: [10.1088/0004-637X/788/1/64](https://doi.org/10.1088/0004-637X/788/1/64)
- Garstang, R. H. 1962, *MNRAS*, 124, 321, doi: [10.1093/mnras/124.4.321](https://doi.org/10.1093/mnras/124.4.321)
- Graney, C. M., & Sarazin, C. L. 1990, *ApJ*, 364, 561, doi: [10.1086/169438](https://doi.org/10.1086/169438)
- Green, W. 2012, *Society for Astronomical Sciences Annual Symposium*, 31, 159
- Gross, J., Williams, B. F., Pannuti, T. G., et al. 2019, *ApJ*, 877, 15, doi: [10.3847/1538-4357/ab189d](https://doi.org/10.3847/1538-4357/ab189d)
- Hatt, D., Beaton, R. L., Freedman, W. L., et al. 2017, *ApJ*, 845, 146, doi: [10.3847/1538-4357/aa7f73](https://doi.org/10.3847/1538-4357/aa7f73)
- Hughes, J. P., Hayashi, I., & Koyama, K. 1998, *ApJ*, 505, 732, doi: [10.1086/306202](https://doi.org/10.1086/306202)
- Humason, M. L., & Wahlquist, H. D. 1955, *AJ*, 60, 254, doi: [10.1086/107223](https://doi.org/10.1086/107223)
- Keenan, F. P., & Norrington, P. H. 1987, *A&A*, 181, 370
- Kewley, L. J., Nicholls, D. C., Sutherland, R., et al. 2019, *ApJ*, 880, 16, doi: [10.3847/1538-4357/ab16ed](https://doi.org/10.3847/1538-4357/ab16ed)
- Kingsburgh, R. L., & Barlow, M. J. 1995, *A&A*, 295, 171
- Lasker, B. M. 1981, *PASP*, 93, 422, doi: [10.1086/130847](https://doi.org/10.1086/130847)
- Lee, H., Grebel, E. K., & Hodge, P. W. 2003, *A&A*, 401, 141, doi: [10.1051/0004-6361:20030101](https://doi.org/10.1051/0004-6361:20030101)

- Lee, M. G., Freedman, W. L., & Madore, B. F. 1993, *ApJ*, 417, 553, doi: [10.1086/173334](https://doi.org/10.1086/173334)
- Leonidaki, I., Boumis, P., & Zezas, A. 2013, *MNRAS*, 429, 189, doi: [10.1093/mnras/sts324](https://doi.org/10.1093/mnras/sts324)
- Levenson, N. A., Kirshner, R. P., Blair, W. P., & Winkler, P. F. 1995, *AJ*, 110, 739, doi: [10.1086/117558](https://doi.org/10.1086/117558)
- Long, K. 2019, in *Supernova Remnants: An Odyssey in Space after Stellar Death II*, 174
- Long, K. S. 2017, in *Handbook of Supernovae*, ed. A. W. Alsabti & P. Murdin (Springer International Publishing AG), 2005, doi: [10.1007/978-3-319-21846-5_90](https://doi.org/10.1007/978-3-319-21846-5_90)
- Long, K. S., Blair, W. P., Milisavljevic, D., Raymond, J. C., & Winkler, P. F. 2018, *ApJ*, 855, 140, doi: [10.3847/1538-4357/aaac7e](https://doi.org/10.3847/1538-4357/aaac7e)
- Long, K. S., Blair, W. P., Winkler, P. F., et al. 2010, *ApJS*, 187, 495, doi: [10.1088/0067-0049/187/2/495](https://doi.org/10.1088/0067-0049/187/2/495)
- Lozinskaya, T. A. 2002, *Astronomical and Astrophysical Transactions*, 21, 223, doi: [10.1080/10556790215592](https://doi.org/10.1080/10556790215592)
- Lozinskaya, T. A., Moiseev, A. V., Afanas'Ev, V. L., Wilcots, E., & Goss, W. M. 2001, *Astronomy Reports*, 45, 417, doi: [10.1134/1.1374637](https://doi.org/10.1134/1.1374637)
- Lozinskaya, T. A., & Podorvanyuk, N. Y. 2009, *Astronomy Letters*, 35, 375, doi: [10.1134/S1063773709060024](https://doi.org/10.1134/S1063773709060024)
- Lozinskaya, T. A., Silchenko, O. K., Helfand, D. J., & Goss, W. M. 1998, *AJ*, 116, 2328, doi: [10.1086/300580](https://doi.org/10.1086/300580)
- Lu, N. Y., Hoffman, G. L., Groff, T., Roos, T., & Lamphier, C. 1993, *ApJS*, 88, 383, doi: [10.1086/191826](https://doi.org/10.1086/191826)
- MacAlpine, G. M., & Satterfield, T. J. 2008, *AJ*, 136, 2152, doi: [10.1088/0004-6256/136/5/2152](https://doi.org/10.1088/0004-6256/136/5/2152)
- MacAlpine, G. M., & Uomoto, A. 1991, *AJ*, 102, 218, doi: [10.1086/115868](https://doi.org/10.1086/115868)
- Maggi, P., Haberl, F., Kavanagh, P. J., et al. 2016, *A&A*, 585, A162, doi: [10.1051/0004-6361/201526932](https://doi.org/10.1051/0004-6361/201526932)
- Martini, P., Stoll, R., Derwent, M. A., et al. 2011, *PASP*, 123, 187, doi: [10.1086/658357](https://doi.org/10.1086/658357)
- Massey, P., Conti, P. S., & Armandroff, T. E. 1987, *AJ*, 94, 1538, doi: [10.1086/114586](https://doi.org/10.1086/114586)
- Massey, P., & Gronwall, C. 1990, *ApJ*, 358, 344, doi: [10.1086/168991](https://doi.org/10.1086/168991)
- Meaburn, J., Clayton, C. A., & Whitehead, M. J. 1988, *MNRAS*, 235, 479, doi: [10.1093/mnras/235.2.479](https://doi.org/10.1093/mnras/235.2.479)
- Melnik, I. A. C., & Copetti, M. V. F. 2013, *A&A*, 553, A104, doi: [10.1051/0004-6361/201220604](https://doi.org/10.1051/0004-6361/201220604)
- Milisavljevic, D., & Fesen, R. A. 2017, in *Handbook of Supernovae*, ed. A. W. Alsabti & P. Murdin (Springer International Publishing AG), 2211, doi: [10.1007/978-3-319-21846-5_97](https://doi.org/10.1007/978-3-319-21846-5_97)
- Millar, W. C., White, G. L., Filipović, M. D., et al. 2011, *Ap&SS*, 332, 221, doi: [10.1007/s10509-010-0556-y](https://doi.org/10.1007/s10509-010-0556-y)
- Murdin, P., Clark, D. H., & Culhane, J. L. 1978, *MNRAS*, 183, 79P, doi: [10.1093/mnras/183.1.79P](https://doi.org/10.1093/mnras/183.1.79P)
- Nazarova, L. S., O'Brien, P. T., & Ward, M. J. 1999, *A&A*, 343, 682. <https://arxiv.org/abs/astro-ph/9901038>
- Nussbaumer, H., & Osterbrock, D. E. 1970, *ApJ*, 161, 811, doi: [10.1086/150585](https://doi.org/10.1086/150585)
- Oke, J. B. 1974, *ApJS*, 27, 21, doi: [10.1086/190287](https://doi.org/10.1086/190287)
- Osterbrock, D. E., & Dufour, R. J. 1973, *ApJ*, 185, 441, doi: [10.1086/152432](https://doi.org/10.1086/152432)
- Osterbrock, D. E., & Ferland, G. J. 2006, *Astrophysics of gaseous nebulae and active galactic nuclei* (University Science Books)
- Ou, P.-S., Chu, Y.-H., Maggi, P., et al. 2018, *ApJ*, 863, 137, doi: [10.3847/1538-4357/aad04b](https://doi.org/10.3847/1538-4357/aad04b)
- Park, S., Hughes, J. P., Slane, P. O., et al. 2012, *ApJ*, 748, 117, doi: [10.1088/0004-637X/748/2/117](https://doi.org/10.1088/0004-637X/748/2/117)
- Patnaude, D., & Badenes, C. 2017, in *Handbook of Supernovae*, ed. A. W. Alsabti & P. Murdin (Springer International Publishing AG), 2233, doi: [10.1007/978-3-319-21846-5_98](https://doi.org/10.1007/978-3-319-21846-5_98)
- Pauletti, D., & Copetti, M. V. F. 2016, *A&A*, 595, A10, doi: [10.1051/0004-6361/201527407](https://doi.org/10.1051/0004-6361/201527407)
- Peimbert, M., Bohigas, J., & Torres-Peimbert, S. 1988, *RMxAA*, 16, 45
- Pietrzyński, G., Gieren, W., Soszyński, I., et al. 2006, *ApJ*, 642, 216, doi: [10.1086/500926](https://doi.org/10.1086/500926)
- Proxauf, B., Öttl, S., & Kimeswenger, S. 2014, *A&A*, 561, A10, doi: [10.1051/0004-6361/201322581](https://doi.org/10.1051/0004-6361/201322581)
- Raymond, J. C. 1979, *ApJS*, 39, 1, doi: [10.1086/190562](https://doi.org/10.1086/190562)
- Raymond, J. C., Edgar, R. J., Ghavamian, P., & Blair, W. P. 2015, *ApJ*, 805, 152, doi: [10.1088/0004-637X/805/2/152](https://doi.org/10.1088/0004-637X/805/2/152)
- Read, A. M., & Pietsch, W. 2001, *A&A*, 373, 473, doi: [10.1051/0004-6361:20010636](https://doi.org/10.1051/0004-6361:20010636)
- Rosado, M. 1986, *A&A*, 160, 211
- Rosado, M., Valdez-Gutiérrez, M., Georgiev, L., et al. 2001, *AJ*, 122, 194, doi: [10.1086/321103](https://doi.org/10.1086/321103)
- Russell, S. C., & Dopita, M. A. 1990, *ApJS*, 74, 93, doi: [10.1086/191494](https://doi.org/10.1086/191494)
- Saha, A., Freedman, W. L., Hoessel, J. G., & Mossman, A. E. 1992, *AJ*, 104, 1072, doi: [10.1086/116298](https://doi.org/10.1086/116298)
- Sandage, A. 1971, *ApJ*, 166, 13, doi: [10.1086/150939](https://doi.org/10.1086/150939)
- Satterfield, T. J., Katz, A. M., Sibley, A. R., MacAlpine, G. M., & Uomoto, A. 2012, *AJ*, 144, 27, doi: [10.1088/0004-6256/144/1/27](https://doi.org/10.1088/0004-6256/144/1/27)
- Sauvageot, J. L., Ballet, J., Dubreuil, D., et al. 1990, *A&A*, 232, 203
- Schlafly, E. F., & Finkbeiner, D. P. 2011, *ApJ*, 737, 103, doi: [10.1088/0004-637X/737/2/103](https://doi.org/10.1088/0004-637X/737/2/103)

- Schlegel, E. M., Pannuti, T. G., Lozinskaya, T., Moiseev, A., & Lacey, C. K. 2019, *AJ*, 158, 137, doi: [10.3847/1538-3881/ab33fb](https://doi.org/10.3847/1538-3881/ab33fb)
- Shull, P., J. 1983, *ApJ*, 275, 592, doi: [10.1086/161558](https://doi.org/10.1086/161558)
- Sibley, A. R., Katz, A. M., Satterfield, T. J., Vanderveer, S. J., & MacAlpine, G. M. 2016, *AJ*, 152, 93, doi: [10.3847/0004-6256/152/4/93](https://doi.org/10.3847/0004-6256/152/4/93)
- Skillman, E. D., Tolstoy, E., Cole, A. A., et al. 2003, *ApJ*, 596, 253, doi: [10.1086/377635](https://doi.org/10.1086/377635)
- Smith, H. E. 1975, *ApJ*, 199, 591, doi: [10.1086/153727](https://doi.org/10.1086/153727)
- Smithsonian Astrophysical Observatory. 2000, SAOImage DS9: A utility for displaying astronomical images in the X11 window environment. <http://ascl.net/0003.002>
- Tuohy, I. R., & Dopita, M. A. 1983, *ApJL*, 268, L11, doi: [10.1086/184020](https://doi.org/10.1086/184020)
- van Dokkum, P. G. 2001, *PASP*, 113, 1420, doi: [10.1086/323894](https://doi.org/10.1086/323894)
- Vancura, O., Blair, W. P., Long, K. S., & Raymond, J. C. 1992, *ApJ*, 394, 158, doi: [10.1086/171567](https://doi.org/10.1086/171567)
- Vogt, F., & Dopita, M. A. 2010, *ApJ*, 721, 597, doi: [10.1088/0004-637X/721/1/597](https://doi.org/10.1088/0004-637X/721/1/597)
- Vogt, F. P. A., Seitzzahl, I. R., Dopita, M. A., & Ghavamian, P. 2017, *A&A*, 602, L4, doi: [10.1051/0004-6361/201730756](https://doi.org/10.1051/0004-6361/201730756)
- Warren, J. S., Hughes, J. P., & Slane, P. O. 2003, *ApJ*, 583, 260, doi: [10.1086/345078](https://doi.org/10.1086/345078)